J. Fluid Mech. (2009), *vol.* 630, *pp.* 93–128.
doi:10.1017/S0022112009006739 Printed in the United Kingdom

Coherent structures in canopy edge flow: a large-eddy simulation study

S. DUPONT† AND Y. BRUNET

INRA, UR 1263, EPHYSE, 71 Avenue Edouard Bourlaux, 33883 Villenave d'Ornon Cedex, France

(Received 10 July 2008 and in revised form 13 February 2009)

Large coherent structures over vegetation canopies are responsible for a substantial part of the turbulent transfer of momentum, heat and mass between the canopy and the atmosphere. As forested landscapes are often fragmented, edge regions may be of importance in turbulent transfer. The development of coherent structures from the leading edge of a forest is investigated here for the first time. For this purpose, the turbulent flow over a clearing–forest pattern is simulated using the Advanced Regional Prediction System (ARPS). In previous studies the code has been modified so as to simulate turbulent flows at very fine scale ($0.1h$, where h is the mean canopy height) within and above heterogeneous vegetation canopies, using a large-eddy simulation (LES) approach. Validations have also been performed over homogeneous forest canopies and over a simple forest–clearing–forest pattern, against field and wind-tunnel measurements. Here, a schematic picture of the development of coherent eddies downstream from the leading edge of a forest is extracted from the mean vorticity components, the Q-criterion field, the cross-correlation of the wind velocity components and the length and separation length scales of coherent structures, determined by using a wavelet transform. This schematic picture shows strong similarities with the development of coherent structures observed in a mixing layer, with four different regions: (i) close to the edge, Kelvin–Helmholtz instabilities develop when a strong wind gust hits the canopy; (ii) these instabilities roll over to form transverse vortices from around $3h$ downstream from the edge, characterized by a length scale close to the depth of the internal boundary layer that develops from the canopy edge; (iii) secondary instabilities destabilize these rollers and increase the vertical and streamwise vorticity components from around $6h$, and two counter-rotating streamwise vortices appear; (iv) at about $9h$ the initial rollers have become complex three-dimensional coherent structures, with spatially constant mean length and separation length scales. These four stages of development occur closer to the edge with increasing canopy density. While this average picture of the development of coherent structures is similar to that observed in a mixing layer, the analysis of instantaneous fields shows that coherent structures behind the leading edge appear as resulting from the 'branching' of tubes localized in regions of low pressure, where their cores are characterized by high values of enstrophy and Q-criterion.

1. Introduction

Turbulent flows can be viewed as composed of coherent eddy structures evolving in unorganized random background turbulence (Schneider & Farge 2003). In the

† Email address for correspondence: sdupont@bordeaux.inra.fr

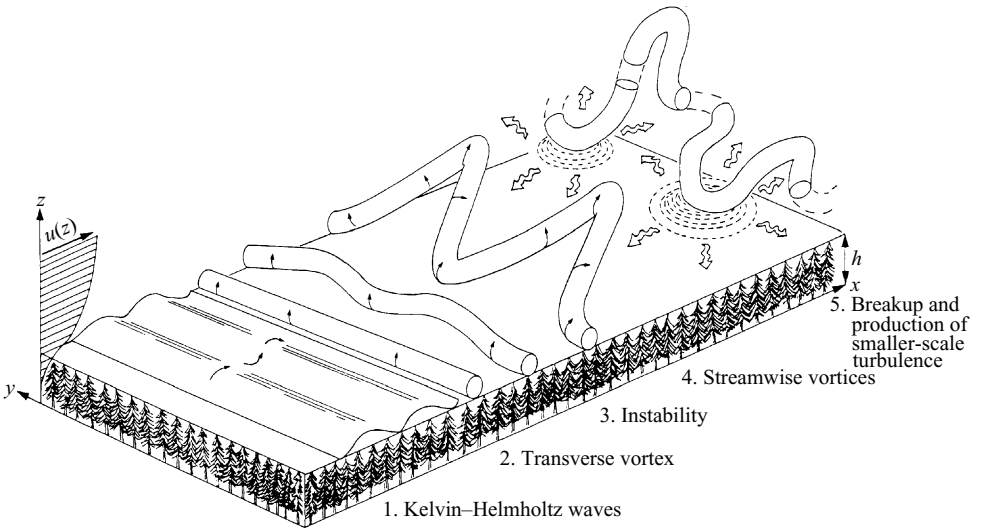

FIGURE 1. Schematic diagram of the formation of coherent eddy structures over a homogeneous canopy, as adapted by Quine *et al.* (1995, p. 24) from Finnigan & Brunet (1995).

natural environment, such coherent structures have been consistently observed over horizontally homogeneous plant canopies. It has been demonstrated that canopy-type structures are generated by processes similar to those occurring in plane mixing-layer flows (Raupach, Finnigan & Brunet 1996), as sketched in the diagram of Finnigan & Brunet (1995) (figure 1). The inflection point in the mean velocity profile at the canopy top leads to the development of Kelvin–Helmholtz instabilities; these instabilities first roll over to form transverse vortices that are subsequently transformed through secondary instabilities into three-dimensional structures. Large coherent structures are characterized by cycles of strong 'sweeps' (gusts) and weak 'ejections' (bursts) that are responsible for a substantial part of the turbulent transfer of momentum, heat and mass between the canopy and the atmosphere (Gao, Shaw & Paw U 1989; Lu & Fitzjarrald 1994). In order to understand transfer processes, a better knowledge of the dynamics of coherent structures is therefore of primary importance. In a broader view, better knowledge is also necessary to improve turbulent flow modelling (Jeong & Hussain 1995). A decomposition of flow fields into active (coherent structures) and inactive components has been advocated as an alternative to the more classical decomposition into average (large-scale) and fluctuating (subgrid-scale or SGS) components (Katul *et al.* 1998; Farge & Schneider 2006).

1.1. *Detection of coherent structures over homogeneous vegetation canopies*

Coherent eddy structures over homogeneous vegetation canopies have been investigated for years from *in situ* and wind-tunnel experiments (Paw *et al.* 1992; Collineau & Brunet 1993*a*, *b*; Turner *et al.* 1994; Qiu, Paw & Shaw 1995; Shaw *et al.* 1995; Brunet & Irvine 2000; Ghisalberti & Nepf 2002) as well as from numerical experiments (Kanda & Hino 1994; Su, Shaw & Paw U 2000; Watanabe 2004; Shaw *et al.* 2006; Dupont & Brunet 2008*b*; Finnigan, Shaw & Patton 2009), as discussed in the next subsection. However, because of their intermittency, their three-dimensional character and the difficulty to isolate them from background turbulence, information on the dynamics and topology of coherent structures still remains limited. Finnigan (2000) reviewed the main techniques used to detect or visualize coherent structures

from experimental time series collected in the vicinity of vegetation canopies. Shaw *et al.* (1995) derived spatial information on these structures by performing space–time correlations on velocity fields measured in a wind tunnel. They observed that turbulent structures are well correlated within a tilted elongated elliptical region extending over $10h$ in the streamwise direction and concentrated in a smaller region of extent about $2h$ in the vertical direction, where h is the canopy height. Unlike in plane mixing-layer flows, these structures progress along the canopy with a convective velocity larger than the mean flow velocity at the canopy top.

Applying empirical orthogonal functions (EOFs) on the dataset of Shaw *et al.* (1995), Finnigan & Shaw (2000) observed that large coherent structures could be represented as a weak ejection followed by a strong sweep in the streamwise direction and as a pair of counter-rotating longitudinal vortices in the spanwise direction. Very recently, Finnigan *et al.* (2009) updated this picture by compositing data from a large-eddy simulation (LES). They observed that head-down hairpin vortices responsible for sweeps are also linked with downstream head-up vortices that induce an ejection upstream from the sweep. In fact, the EOF-derived structure is the ensemble average of the two hairpin vortices (Finnigan *et al.* 2009).

Since the presence of coherent structures can be identified from occasional large-amplitude excursions of instantaneous flow variables from their mean values, several conditional techniques have also been used in the literature to detect ramp-like coherent structures in time series of turbulent variables (see Finnigan 2000 for a short review). Conditional sampling techniques are easier to use than two-point space–time correlations, since they do not require simultaneous measurements at different locations. The wavelet transform is one of these techniques that has already demonstrated its ability (Collineau & Brunet 1993*a*, *b*; Turner *et al.* 1994; Qiu *et al.* 1995; Brunet & Irvine 2000). Collineau & Brunet (1993*a*, *b*) were the first to demonstrate that the wavelet transform is a suitable tool for detecting coherent structures in the vicinity of vegetation canopies by decomposing time series into time and space and by determining the location of the dominant structures in the time series. Using such techniques and others, Raupach *et al.* (1996) showed that the mean longitudinal separation between adjacent coherent structures is a function of a shear length scale derived from the vorticity thickness of plane mixing layers, and Brunet & Irvine (2000) extended these results to a larger dataset including non-neutral atmospheric conditions.

1.2. *LES over vegetation canopies*

Direct numerical simulation (DNS) and LES provide details of the velocity field, allowing the spatial characteristics of large turbulent structures to be analysed, since instantaneous dynamic fields are explicitly resolved at a resolution not attainable in field or wind-tunnel experiments. DNS and LES have been widely used by the fluid mechanics community to analyse the development and topology of coherent structures in wall-bounded flows or in other flow configurations such as mixing layers (see, for example, Comte, Lesieur & Fouillet 1989; Comte, Lesieur & Lamballais 1992; Dubief & Delcayre 2000; Lesieur *et al.* 2003; Schneider *et al.* 2005). In the same way as for field and wind-tunnel experiments, one of the main difficulties encountered in these studies concerns the extraction of coherent structures from background turbulence. A coherent structure is usually considered as a vortex, but the concept of a vortex is still ambiguous (Jeong & Hussain 1995; Cucitore, Quadrio & Baron 1999; Haller 2005). For this purpose, several identification techniques of vortex cores have been developed, focusing on regions of low pressure or large vorticity or on the eigenvalues

of the velocity-gradient tensor. Reviews of these techniques are presented in Jeong & Hussain (1995) and Cucitore *et al.* (1999), who showed that they are all prone to fail in specific conditions. For example the vorticity magnitude, i.e. the enstrophy, does not appear as an adequate criterion for the identification of vortices in shear flows in which the flow rotation rate is comparable to the strain rate (Jeong & Hussain 1995). Indeed, vorticity can be large in parallel shear flow without the presence of vortices (Haller 2005). Therefore, vortex cores are usually defined as regions in which the rotation rate dominates the strain rate, known also as roller regions, in opposition to the braid region in which the strain rate dominates the rotation rate (Rogers & Moser 1994).

Over homogeneous vegetation canopies the LES approach has first been applied in neutral stratification by Shaw & Schumann (1992), who obtained qualitative agreement with mean turbulence statistics derived from *in situ* and wind-tunnel datasets. Further studies confirmed that LES is able to reproduce in detail many observed characteristics of turbulent flow over homogeneous canopies (Kanda & Hino 1994; Dwyer, Patton & Shaw 1997; Shen & Leclerc 1997; Su *et al.* 1998, 2000; Watanabe 2004; Dupont & Brunet 2008*b*). Coherent structures from resolved LES flow fields have been analysed by several authors. Kanda & Hino (1994) obtained a picture of an instantaneous coherent structure similar to that observed *in situ* by Gao *et al.* (1989). Su *et al.* (2000) showed that two-point correlation fields can reproduce the main characteristics observed *in situ* and in a wind tunnel, and Watanabe (2004) analysed coherent eddy structures from ensemble-averaged scalar ramp structure detection. Dupont & Brunet (2008*b*) studied the impact of the vertical variation in leaf area index (LAI, the total leaf area per unit surface area) on the characteristics of coherent structures. To date, the most detailed numerical study on coherent eddies over homogeneous canopies has been performed by Finnigan *et al.* (2009), who characterized the structure of coherent eddies from a composite average deduced from LES outputs.

Turbulent flows over forest edges and clearings have been studied in several wind-tunnel (Raupach, Bradley & Ghadiri 1987; Chen, Novak & Adams 1995) and field (Raynor 1971; Gash 1986; Irvine, Gardiner & Hill 1997; Flesch & Wilson 1999; Nieveen, El-Kilani & Jacobs 2001) experiments. Lee (2000) presented a review of studies on disturbed flow across forest edges. The edge flow can be divided into several distinct regions as suggested by Belcher, Jerram & Hunt (2003) in their analytical model: (i) the impact region at the edge; (ii) the adjustment region behind the edge, where the flow adjusts with the canopy; (iii) the canopy interior region further downstream, where the flow has adjusted with the canopy characteristics; (iv) the canopy shear layer at the canopy top, where coherent structures develop; and (v) the roughness-change region representing the growing internal boundary layer (IBL), which develops above the canopy. LES has also been applied to heterogeneous vegetation canopies by several authors but without focusing on coherent structures. Patton *et al.* (1998) validated their model in a configuration with multiple windbreaks against the wind-tunnel dataset of Judd, Raupach & Finnigan (1996). Yang *et al.* (2006*a*, *b*) analysed momentum and turbulent kinetic energy (TKE) budgets, and Dupont & Brunet (2008*a*) analysed the structure of the flow in the edge region for various vertical distributions of leaf area. Additionally, Cassiani, Katul & Albertson (2008) investigated the main characteristics of the flow behind forest trailing edges.

1.3. *Objectives*

The objective of the present work is to analyse the development of coherent structures from the leading edge of sparse and dense forest canopies in a neutral and

dry atmosphere. For this purpose, LES fields were computed with the Advanced Regional Prediction System (ARPS) version 5.1.5, developed at the Center for Analysis and Prediction of Storms (CAPS) at the University of Oklahoma and modified by Dupont & Brunet (2008*b*) to simulate turbulent flows over plant canopies at very fine scales (about $0.1h$, where h is the mean canopy height). The average velocity and the turbulent statistical fields simulated by this new version of the ARPS have already been validated against field and wind-tunnel measurements over homogeneous forest canopies, in a simple forest–clearing–forest transition, as well as over a forested hill (Dupont & Brunet 2008*a*,*b*; Dupont, Brunet & Finnigan 2008).

The model is first presented, along with the numerical simulation set-up and the procedures used to analyse field data. We then analyse the mean statistical turbulence fields across the forest edge and the development of coherent structures from the leading edge as deduced from mean enstrophy and Q-criterion fields. We later perform a two-point space correlation analysis and a conditional analysis of the velocity fields. The development of specific coherent structures from instantaneous turbulence fields are then investigated, before we move on to the final discussion.

2. Methods

2.1. *Model*

The ARPS is a complete weather forecast system that has been extensively validated over the last decade in a variety of mesoscale flows. A detailed description of the standard version of the model and the results of validation exercises are available in the ARPS user's manual (Xue *et al.* 1995) and in Xue, Droegemeier & Wong (2000) and Xue *et al.* (2001). We describe here briefly the model, with a focus on the modifications that were made in order to simulate the flow within vegetation canopies.

The ARPS is a three-dimensional, non-hydrostatic compressible model in which Navier–Stokes equations are written in terrain-following coordinates. The grid is orthogonal in the horizontal direction and stretched in the vertical. The model solves the conservation equations for the three wind velocity components, pressure, potential temperature and water substance (water vapour, cloud water, rainwater, cloud ice, snow and graupel). Each wind component and atmospheric state variable (air density, pressure and potential temperature) is split into a base-state component (overbarred variable) and a deviation from the latter (double-primed variable). The base state is assumed to be horizontally homogeneous, time invariant and hydrostatically balanced. To ensure high spatial resolution, all conservation equations are filtered so as to separate the small scales from the large scales. Large eddies are therefore explicitly resolved by the equations, while the effect of smaller eddies on larger eddies is modelled. The discretization of the equations on the grid is treated as an implicit filter operation. Therefore, filtered equations can be seen as grid-volume-averaged equations. Within the vegetated layer, the shear flow at the canopy top involves eddies larger than wake eddies behind vegetation elements, and dissipation occurs through the smallest eddies (down to the Kolmogorov scale). The filter scale or grid spacing is located within the inertial sub-range. All turbulent structures larger than the filter scale are explicitly resolved by the model; this is the case for most turbulent eddies produced by wind shear, while smaller turbulent structures, i.e. SGS turbulent motions, are modelled through a 1.5-order turbulence closure scheme with the resolution of a conservation equation for SGS TKE.

The ARPS momentum and SGS TKE equations have been modified so as to account for the effect of vegetation on the turbulent flow in the same manner as Watanabe (2004). For the sake of simplicity momentum and SGS TKE equations presented hereafter are written in Cartesian coordinates for a dry atmosphere, and all simulations presented here are only performed under neutrally stratified and dry flow over a flat terrain. Despite the atmosphere being considered as neutral, heat terms are present in these equations, since the potential temperature equation (not shown) is solved to provide initial turbulent perturbations leading to the development of turbulent motions. Using the Einstein summation convention the momentum equation for a Boussinesq fluid is therefore written as

$$\overline{\rho}\left(\frac{\partial \widetilde{u_i}}{\partial t}+\widetilde{u_j}\frac{\partial \widetilde{u_i}}{\partial x_j}\right)=-\frac{\partial}{\partial x_i}\left(\widetilde{p}''-\alpha_{div}\frac{\partial \overline{\rho}\widetilde{u_j}}{\partial x_j}\right)-2\overline{\rho}\omega_j\epsilon_{ijk}(\widetilde{u_k}-\overline{u_k})$$
$$-\overline{\rho}g\left(\frac{\widetilde{\theta}''}{\overline{\theta}}-\frac{c_p}{c_v}\frac{\widetilde{p}''}{\overline{p}}\right)\delta_{i3}-\overline{\rho}\frac{\partial \boldsymbol{\tau}_{ij}}{\partial x_j}-C_d A_f\sqrt{\widetilde{u_j}\widetilde{u_j}}\widetilde{u_i}, \quad (2.1)$$

where the overtilde indicates the filtered variables or grid-volume-averaged variables. In this equation, t is time and x_i $(x_1=x, x_2=y, x_3=z)$ are the streamwise, lateral and vertical directions, respectively; u_i $(u_1=u, u_2=v, u_3=w)$ are the instantaneous velocity components along x_i; δ_{ij} is the Kronecker symbol; ϵ_{ijk} is the alternating unit tensor; α_{div} is a damping coefficient used to attenuate acoustic waves; p is the air pressure; ρ the air density; g the acceleration due to gravity; θ the potential temperature; and c_p and c_v are the specific heat of air at constant pressure and volume, respectively.

The terms on the right-hand side of (2.1) represent respectively the pressure-gradient force term, the Coriolis term, the buoyancy term, the turbulent transport term and the pressure and viscous drag force term induced by the vegetation; C_d is the mean drag coefficient of the canopy and A_f is the frontal area density of the vegetation (m^2m^{-3}). In the Coriolis term, ω represents the angular velocity of the Earth, and the second part of the Coriolis term, $-2\overline{\rho}\omega_j\epsilon_{ijk}\overline{u_k}$, represents the geostrophic pressure-gradient force associated with the base-state wind. The Coriolis force is only applied on wind perturbations, since the steady base state is already geostrophically balanced.

The Reynolds or sub-filter-scale or subgrid stress tensor $\boldsymbol{\tau}_{ij}$ is modelled through an SGS eddy-viscosity or gradient-transport model as

$$\boldsymbol{\tau}_{ij}=-\nu_t\left(\frac{\partial \widetilde{u_i}}{\partial x_j}+\frac{\partial \widetilde{u_j}}{\partial x_i}\right), \quad (2.2)$$

where ν_t is the eddy viscosity modelled as the product of a length scale and a velocity scale characterizing the SGS turbulent eddies, following

$$\nu_t=0.1\sqrt{e}\,l. \quad (2.3)$$

In a neutral atmosphere with isotropic turbulence, the mixing length depends on the grid spacing:

$$l=(\Delta x\Delta y\Delta z)^{1/3}, \quad (2.4)$$

where Δx, Δy and Δz are the grid spacings in the longitudinal, lateral and vertical directions, respectively. In the ARPS it is also possible to use different horizontal and vertical mixing lengths for different horizontal and vertical grid spacings.

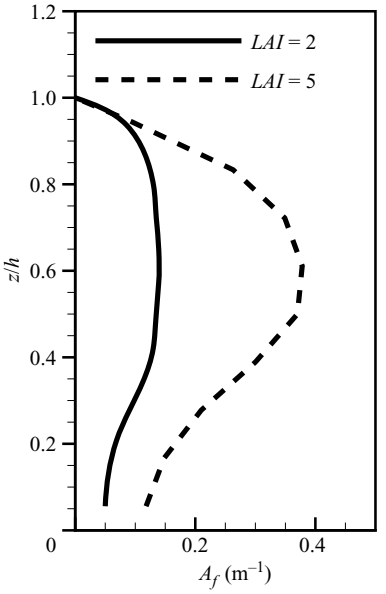

FIGURE 2. Frontal area density profiles of the two forest canopies considered here.

The SGS velocity scale is computed by solving the conservation equation of the SGS TKE e:

$$\frac{\partial e}{\partial t} + \widetilde{u}_j \frac{\partial e}{\partial x_j} = -\tau_{ij} \frac{\partial \widetilde{u}_i}{\partial x_j} - \frac{g}{\overline{\theta}} \tau_{3\theta} + \frac{\partial}{\partial x_j} \left(2\nu_t \frac{\partial e}{\partial x_j} \right) - C_\epsilon \frac{e^{3/2}}{l} - 2C_d A_f \sqrt{\widetilde{u}_j \widetilde{u}_j} e. \quad (2.5)$$

The terms on the right-hand side of (2.5) represent respectively the dynamic shear production term, the buoyancy production term, the turbulent transport term, the dissipation term and the SGS TKE cascade term; the last term represents the energy-loss process that accelerates the dissipation of turbulence in the canopy – as the eddies of all scales larger than the canopy elements lose their TKE to both heat and wake through their interaction with the vegetation, the inertial eddy cascade is short-circuited (Baldocchi & Meyers 1988; Finnigan 2000). This is emphasized by the presence of small wake eddies. The SGS TKE production by wake motions behind vegetation elements is not considered, as their scales are much smaller than those making up the bulk of SGS TKE (Shaw & Schumann 1992).

The subgrid heat flux is written as

$$\tau_{3\theta} = -\frac{\nu_t}{P_r} \frac{\partial \widetilde{\theta}}{\partial x_3}, \quad (2.6)$$

where the Prandtl number P_r is taken equal to 1 in the present study.

For the sake of simplicity the overtilde on $\widetilde{u}_i$ will be omitted from now on.

2.2. *Numerical details*

Two three-dimensional simulations have been performed over a canopy–clearing–canopy pattern in which the canopy height, h, is set at 18 m with a frontal area density, A_f, corresponding to the deciduous forest studied by Shaw, Hartog & Neumann (1988). Two cases of LAI are considered: $LAI = 2$ and 5 for cases 1 and 2, respectively (see figure 2). These two values of LAI should provide relevant information on the impact of variations in canopy density on turbulent edge flow

fields, without considering extreme cases, as in nature plant canopy LAI ranges from 1.3 ± 0.9 for deserts to 8.7 ± 4.3 for tree plantations (Asner, Scurlock & Hicke 2003). The drag coefficient, C_d, is equal to 0.2, which is a typical value often observed for trees. The clearing and forest lengths are set to $20h$ and $17.1h$, respectively. As lateral boundary conditions are periodic, these clearing and forest lengths result from a compromise between constraints related to the available computational time, to a canopy length that is large enough for observing flow adjustment with the forest canopy and to a clearing length that is large enough for limiting the impact of the upwind forest on the leading-edge flow. Note that the length of the clearing chosen here is similar to that used in previous wind-tunnel (Raupach *et al.* 1987) and LES (Yang *et al.* 2006*b*; Dupont & Brunet 2008*b*) studies also related to forest edge flow.

The computational domain extends over $668 \times 200 \times 200\,\mathrm{m}^3$, corresponding to $345 \times 100 \times 65$ grid points in the x-, y- and z-direction, respectively, with 2 m grid spacing below $z = 84$ m and a vertically stretched grid above. This resolution allows us to simulate turbulent structures induced by the mean shear at the canopy top, since their horizontal size is of the order of h, and their vertical size of the order of $h/3$ (Finnigan 2000). The limitation of the vertical size of the domain due to computational time considerations does not allow large mesoscale structures to be resolved. This should not have noticeable consequences on the main results of this study, which only focuses on turbulence at the canopy scale, in a neutral atmosphere.

The lateral boundary conditions are periodic. At the lower boundary, treated as a rigid surface, the momentum flux is parameterized using a bulk aerodynamic drag law. A 70 m depth Rayleigh damping layer is used at the upper boundary in order to absorb upward-propagating wave disturbances and to eliminate wave reflection at the top of the domain. The velocity fields are initialized from the base-state wind profile which was computed from a meteorological pre-processor (Pénelon, Calmet & Mironov 2001) with a constant vertical profile of potential temperature (300 K), a dry atmosphere and geostrophic wind components equal to $18\,\mathrm{m\,s^{-1}}$ and $-3.5\,\mathrm{m\,s^{-1}}$ in the x- and y-direction, respectively. The flow is driven by the geostrophic pressure gradient associated with the base-state wind in the Coriolis term (2.1).

2.3. *LES data analysis*

After the flow has reached an equilibrium state, wind velocity and turbulent statistical fields are averaged in space over all y-locations at all given heights z and in time over 90 samples collected during a 30 min period. Consequently, wind velocity components u_i can be decomposed into $u_i = \langle u_i \rangle_{yt} + u_i'$, where the symbol $\langle\rangle_{yt}$ denotes the time and space average and the prime the deviation from the averaged value. For convenience in the result analysis, the origin of the longitudinal axis is hereafter set at the forest leading edge.

The following variables are selected to describe the turbulent statistics:

(i) The total mean TKE $k_{tot} = 1/2\langle u_i' u_i' \rangle_{yt} + \langle e \rangle_{yt}$, which includes the resolved and SGS components of TKE.

(ii) The vertical momentum flux $\langle u'w' \rangle_{yt}$.

(iii) The ratio between the Reynolds stresses in the fourth and second quadrants, $Q_{uw} = \langle u'w' \rangle_{yt}^{IV} / \langle u'w' \rangle_{yt}^{II}$, corresponding to sweep and ejection events, respectively. This parameter allows the overall relative contribution of the ejection and sweep eddy motions to the mean momentum flux to be quantified.

(iv) The correlation coefficient between u and w, representing the efficiency of turbulence for momentum transport, $r_{uw} = \langle u'w' \rangle_{yt} / \sigma_u \sigma_w$, where σ_{u_i} is the standard deviation of the velocity component u_i.

(v) The pressure variance $\langle p'^2 \rangle_{yt}$.

(vi) The skewness of u_i, $Sk_i = \langle u_i'^3 \rangle_{yt} / \langle u_i' u_i' \rangle_{yt}^{3/2}$, which provides information about the symmetry of the probability distribution of u_i around its mean value.

(vii) The two-point cross-correlation coefficients, computed from the velocity components at various distances X from the canopy leading edge, so as to characterize the mean size of coherent eddy structures,

$$R_{ij}(x - X, y, z) = \frac{\langle u_i(X, 0, h) u_j(x, y, z) \rangle_t}{\sigma_{u_i}(X, 0, h) \sigma_{u_j}(x, y, z)}, \tag{2.7}$$

where the reference point of the correlation is located at distance X from the canopy leading edge, at the origin of the lateral coordinates (middle of the lateral side of the computational domain) and at the canopy top. When R_{ij} is analysed in the x–z plane, it is spatially averaged over all y-locations at each considered $(x - X, z)$-position, in addition to time averaging.

(viii) The local rotation rate of the flow, quantified from the enstrophy, i.e. half the square of relative vorticity,

$$E = 1/2 \langle \omega_i \omega_i \rangle_{yt}, \tag{2.8}$$

where ω_i is the instantaneous vorticity component of the flow along x_i.

(ix) The Q-criterion, which quantifies the relative amplitude of the rotation rate and the strain rate of the flow and helps identify vortex cores,

$$Q_c = 1/2 \langle \boldsymbol{\Omega}_{ij} \boldsymbol{\Omega}_{ij} - \boldsymbol{S}_{ij} \boldsymbol{S}_{ij} \rangle_{yt}, \tag{2.9}$$

where $\boldsymbol{\Omega}_{ij} = (u_{i,j} - u_{j,i})/2$ and $\boldsymbol{S}_{ij} = (u_{i,j} + u_{j,i})/2$ are the antisymmetric and symmetric components of the velocity-gradient tensor, respectively (where the subscript 'comma' denotes partial differentiation). The Q-criterion is expected to be positive in vortex cores.

Additionally, the length and separation length scales of coherent structures at the canopy top are assessed at several distances from the leading edge from the wavelet transform technique applied on 30 min time series of the streamwise and vertical velocities by using the same procedure as that given by Brunet & Irvine (2000). A summary of this procedure is provided in the Appendix.

3. Results

The conventional mean turbulent fields are first analysed over the forest leading edge. Several of these fields have already been validated over a forest edge by Dupont & Brunet (2008*a*) against the wind-tunnel measurements of Raupach *et al.* (1987), and the spatial length and frequency of simulated coherent structures have also been validated over homogeneous canopies (Dupont & Brunet 2008*b*). We can therefore be confident in the ability of the ARPS to simulate coherent structures accurately. In the following subsections, the development of coherent structures from the leading edge is investigated through the mean enstrophy (2.8) and Q-criterion (2.9) fields, the cross-correlation of wind velocity components (2.7) and the separation length scale of the structures. Finally, the observation of instantaneous turbulent fields allows us to follow the various stages of development of two specific coherent structures.

3.1. *Mean statistical fields across a canopy edge*

Figure 3 presents x–z slices of time- and y-averaged $\langle u \rangle_{yt}$, $\langle w \rangle_{yt}$, k_{tot}, $\langle u'w' \rangle_{yt}$, Q_{uw}, r_{uw}, $\langle p'^2 \rangle_{yt}$ and Sk_u across the forest edge with $LAI = 2$. Here $\langle u \rangle_{yt}$, $\langle w \rangle_{yt}$, k_{tot}, $\langle u'w' \rangle_{yt}$

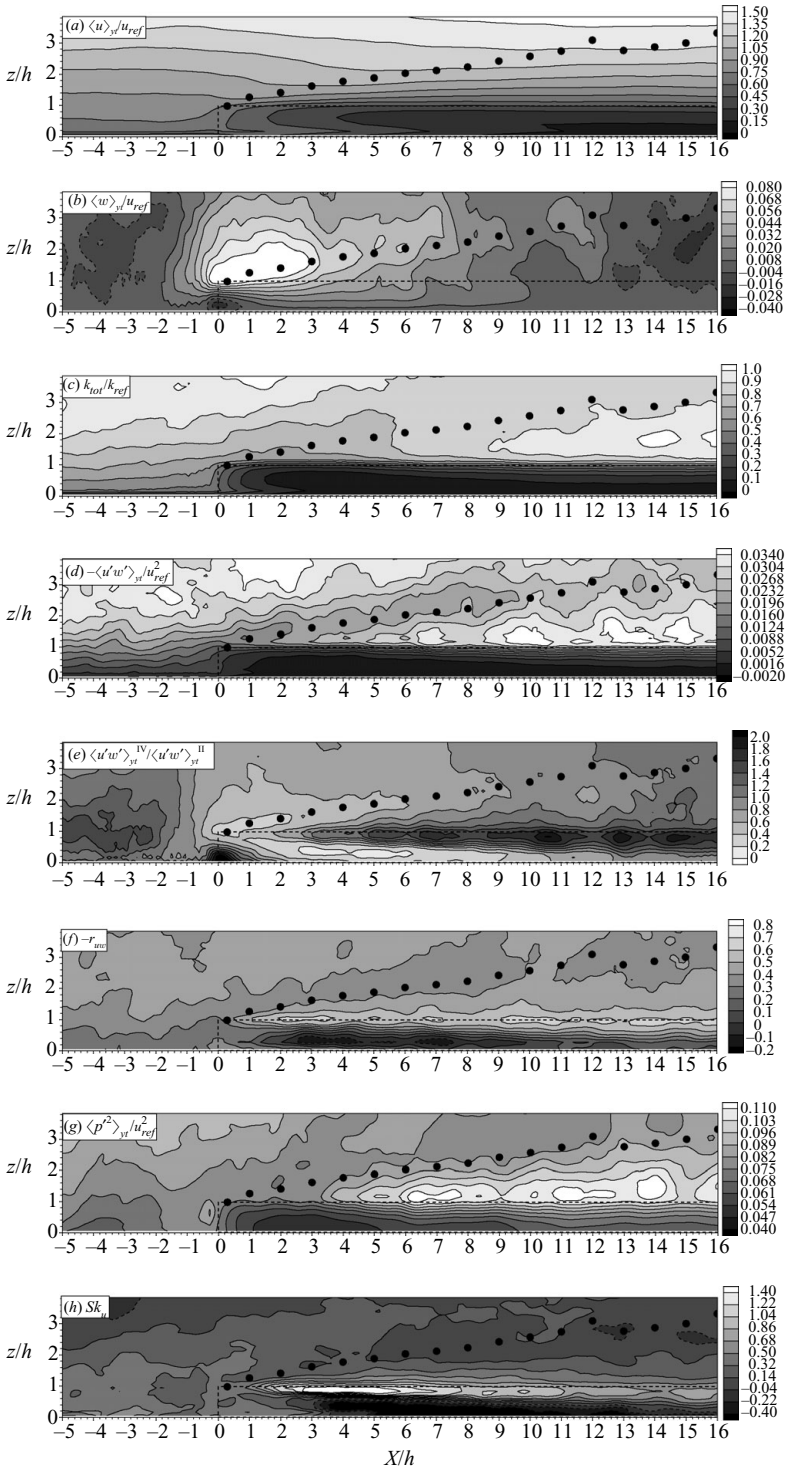

FIGURE 3. Vertical cross-section of the average simulated edge flow in case 1 ($LAI = 2$): streamwise wind velocity (a), vertical velocity (b), TKE (c), momentum flux (d), ratio of the Reynolds stresses in the fourth and second quadrants (e), correlation coefficient (f), pressure variance (g) and skewness of u (e). All variables are normalized from mean quantities computed at $X = -8.5h$ and $z = 2h$. The dashed black line indicates the contour of the canopy and the black dots the upper limit of the IBL.

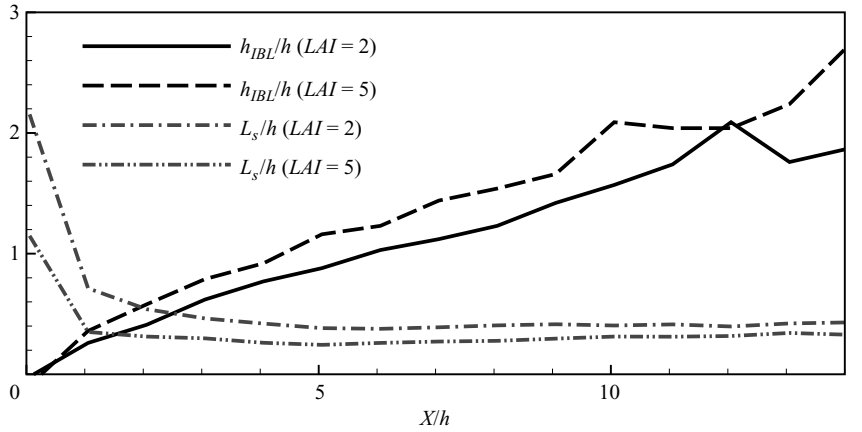

FIGURE 4. Variation of the IBL depth, h_{IBL}, and the shear length scale, L_s, downwind from the forest leading edge in cases 1 ($LAI = 2$) and 2 ($LAI = 5$).

and $\langle p'^2 \rangle_{yt}$ are normalized with the streamwise velocity u_{ref} located upwind from the forest leading edge, at $X = -8.5h$ and $z = 2h$. Before we analyse the flow behind the edge, it is convenient to briefly describe the flow in the clearing. Downwind from the trailing edge of the first forest block, at $X = -20h$, the flow accelerates near the ground and starts to adjust with the new surface underneath (not shown). The large amount of TKE around treetop is advected downwind from the first forest block and diffuses over the vertical, as for momentum, characterizing the wake region of the upwind forest. Although figure 3 focuses on the leading-edge flow of the second forest block, this wake region is visible on the upper left of figure 3(c, d) at $X = -5h$, where TKE and the momentum flux are larger at $z = 3h$ than when closer to the ground. In the clearing the flow progressively reaches a new equilibrium with the surface. The length of the clearing, $20h$, is not sufficient for a fully adjusted flow to be observed, but it is large enough to limit the impact of the wake region of the upwind forest on the leading-edge flow.

As for a surface roughness transition, the flow at the forest leading edge is distorted, and an IBL develops above the canopy, while the flow adjusts with the canopy underneath. As will be seen further, this adjustment does not start at the edge but after a few canopy heights downstream, defining the adjustment region that precedes the equilibrium region. Several methods exist to estimate the IBL height, as reviewed by Bou-Zeid, Meneveau & Parlange (2004). The IBL depth h_{IBL} is computed here as the height above the canopy at which the averaged wind profile becomes insensitive to the canopy underneath, i.e. $\partial \langle u \rangle_{yt} / \partial z = \partial \langle u \rangle_{xyt} / \partial z$, where $\langle \rangle_{xyt}$ indicates a time and spatial average along the streamwise and spanwise directions. The IBL growth is shown in figure 4 through the variation of the IBL depth, h_{IBL}, from the edge; the upper limit of the IBL is also shown with black dots in figure 3. It appears from figure 4 that h_{IBL} increases rapidly from the edge, then reaches about $1h$ above the canopy at $X = 6h$ and is still growing at $X = 16h$.

The adjustment region is characterized by a decrease in horizontal velocity within the forest downwind from the edge (figure 3a) and a positive vertical velocity (figure 3b). A streamwise wind jet forms in the sub-canopy layer from the leading edge to about $X = 10h$, due to the lower density of the canopy trunk layer as compared to the crown layer. Above the canopy the flow accelerates, and the vertical

velocity remains positive down to about $X = 10h$. There the streamwise flow velocity has adjusted with the canopy, and the vertical component is virtually zero. Belcher, Finnigan & Harman (2008) attempted to estimate the length of the adjustment region from basic canopy properties (drag coefficient, C_d, and frontal area density, A_f). They deduced from an analytical approach of a neutrally stratified edge flow that there should be an adjustment region about $3L_c$ in length, where L_c is the adjustment length scale for momentum defined as $L_c = h/\int_0^h C_d A_f \mathrm{d}z$. This estimate was in agreement with measurements performed over model trees and arrays of cubes and cylinders (Belcher *et al.* 2008). In the present study, if we assume that the adjustment region ends where $\langle w \rangle_{yt}/u_{ref} < 0.01$ at the canopy top, its length is about $10h$, which represents about $4L_c$. This is a result similar to that of Belcher *et al.* (2008), with a slightly larger distance that may be due to the fact that L_c is assumed to depend only on the integral value of foliage canopy properties and thus does not include the vertical distribution of the foliage. Here, the presence of a streamwise wind jet within our sub-canopy layer may be responsible for the longer adjustment region, compared to a canopy with a uniform vertical foliage distribution.

A shear layer forms at the canopy top, defined by a strong wind shear and an inflected wind profile. The depth of this layer is usually characterized by the shear length scale L_s defined by Raupach *et al.* (1996) as $L_s = \langle u \rangle_{yt}^{z=h}/(\partial \langle u \rangle_{yt}/\partial z)_{z=h}$. The canopy-top shear layer adjusts rapidly from the edge, as L_s reaches its equilibrium value of $0.38h$ at about $X = 3h$ (figure 4). Slightly further downstream, the large wind shear at treetop induces the development of a region of strong turbulence above the canopy from around $X = 8h$, visible in figure 3(*c*) as a growing sublayer within the IBL. As previously observed (see, for example, Liu *et al.* 1996; Morse, Gardiner & Marshall 2002; Dupont & Brunet 2008*a*), the production of turbulence is not effective from the leading edge but coincides with the vertical velocity approaching zero, as was suggested by Morse *et al.* (2002). Indeed, while the contribution of streamwise advection to the TKE budget is only significant in the region just behind the leading edge, the contribution of vertical advection is significant in the whole adjustment region, from $X = 0h$ to $X = 10h$, in agreement with the behaviour of vertical velocity. This contribution goes through a maximum in the region $X = 2h$–$3h$, where TKE is minimum and where the contribution of SGS TKE is maximum (up to 8 % of total TKE; result not shown). Although TKE is produced by the shear layer at the canopy top, the vertical advection of TKE explains the delay in the development of the turbulent region above the canopy, due to the advection of less turbulent flow from the lowest layers towards the top of the canopy. Further downstream, in the equilibrium region, TKE at the canopy top is essentially produced by vertical shear and partially dissipated by canopy drag, while the turbulent diffusion term is a sink for TKE above the canopy and a source within the canopy (Yang *et al.* 2006*a*). This implies that TKE is imported within the canopy from above through the action of coherent structures, which maintains a significant level of TKE in the lower canopy through pressure diffusion.

The vertical momentum flux decays very rapidly within the canopy, and a region of large flux develops above the canopy, within the IBL and closer to the edge than for TKE (figure 3*d*). Just behind the edge, a small region with a positive (upward) momentum flux is present within the canopy (not visible in the figure). This feature may be explained by a mean upward motion due to the decrease of wind velocity in the canopy. Up to about $X = 3h$ downwind from the edge, momentum transfer is dominated by ejection motions (figure 3*e*), whereas further downstream sweep motions become large, as is observed over homogeneous canopies (Raupach *et al.*

1996; Finnigan 2000). At the canopy top, the correlation coefficient r_{uw}, a measure of the efficiency of transport by turbulence, is fairly low at the edge (about -0.28) and increases rapidly further downwind to reach its equilibrium value, about -0.55, around $X = 2h$ (figure 3*f*). In the same way as the shear length scale, L_s, at the canopy top, r_{uw} adjusts very rapidly with the canopy in comparison with other turbulent variables. This behaviour of r_{uw} as well as its magnitude is fairly consistent with those reported by Morse *et al.* (2002) from field and wind-tunnel experiments. While the lower values of r_{uw} at the edge may be explained by the absence of canopy-scale eddies, as suggested by Morse *et al.* (2002), the rapid increase and adjustment of r_{uw} further downstream is not quite clear, as canopy-scale eddies may only develop from around $X = 2h$ (see § 3.2).

The pressure variance increases from $X = 3h$ and seems adjusted around $X = 6h$. It shows a maximum just above the canopy (figure 3*g*). Within the upper canopy, between $z = 0.7h$ and $z = 1h$ and between $X = 2.5h$ and $X = 6h$, a region of large skewness in streamwise velocity ($Sk_u > 1.5$) is simulated, indicating an asymmetric distribution of wind velocity around its mean value, with a larger probability of sudden strong events (gusts). This region corresponds to the 'enhanced gust zone' (EGZ) observed by Raupach *et al.* (1987) between $X = 3h$ and $X = 7h$ and from $z = 0.6h$ to the canopy top, centred around $X = 5h$ and $z = 0.8h$. Further downstream, Sk_u decreases to about 0.5, as is usually observed over homogeneous canopies (Raupach *et al.* 1996; Finnigan 2000). This EGZ is located in the region in which TKE is small, upstream of the growing TKE sublayer. Dupont & Brunet (2008*a*) suggested that the presence of the EGZ may be caused by the fact that the low turbulence levels in this region emphasize the appearance of strong wind gusts coming from aloft or from the clearing, thereby increasing the skewness of the flow. Further downstream strong wind gusts are more 'diluted' in larger ambient turbulence. In the lower canopy, a region with $Sk_u < 0$ develops from about $X = 3h$, just below the EGZ. This region becomes less deep further downstream but still exists close to the ground. Despite the average upward motion of the flow above the canopy leading edge, Sk_w is characterized by large negative values just behind the edge (figure not shown), indicating the presence of strong intermittent downward motions. Further downstream, Sk_w reaches typical negative values observed within homogeneous canopies.

With a denser canopy ($LAI = 5$), the deceleration of the flow within the canopy is enhanced, inducing a larger flow distortion at the leading edge, visible through the larger positive vertical velocity (figure 5) and a faster growing IBL (figure 4). As turbulence within the IBL increases with canopy density, the faster growth rate of the IBL is in agreement with the usual scaling argument that considers the IBL growth rate $\mathrm{d}h_{IBL}/\mathrm{d}X$ to be of the order of $\langle w'^2\rangle_{yt}^{1/2}/\langle u(h_{IBL})\rangle_{yt}$, where $\langle w'^2\rangle_{yt}^{1/2}$ is the standard deviation of the vertical velocity within the IBL and $\langle u(h_{IBL})\rangle_{yt}$ the mean streamwise velocity at the IBL top. A weak wind jet is still present in the trunk space just behind the edge. The region of higher r_{uw} is located closer to the edge than in the sparser canopy case. In the same way, the pressure variance is larger and starts to increase closer to the edge, from about $X = 2h$ against $X = 3h$ in case 1. The EGZ extends from $X = 1.5h$ to $X = 5h$ against $X = 3h$–$5.5h$, and the shear length scale, L_s, has adjusted at $X = 1h$ against $X = 5h$ (figure 4). Consequently, a denser canopy leads to more active turbulence processes in the adjustment region and a more rapid adjustment of the flow after the edge. (The length of the adjustment region is about $8h$ with $LAI = 5$ against $10h$ with $LAI = 2$.) This latter feature is consistent with the parameterization of the adjustment length scale, L_c, suggested by Belcher *et al.* (2008), which implies that L_c decreases with increasing canopy density. However, the

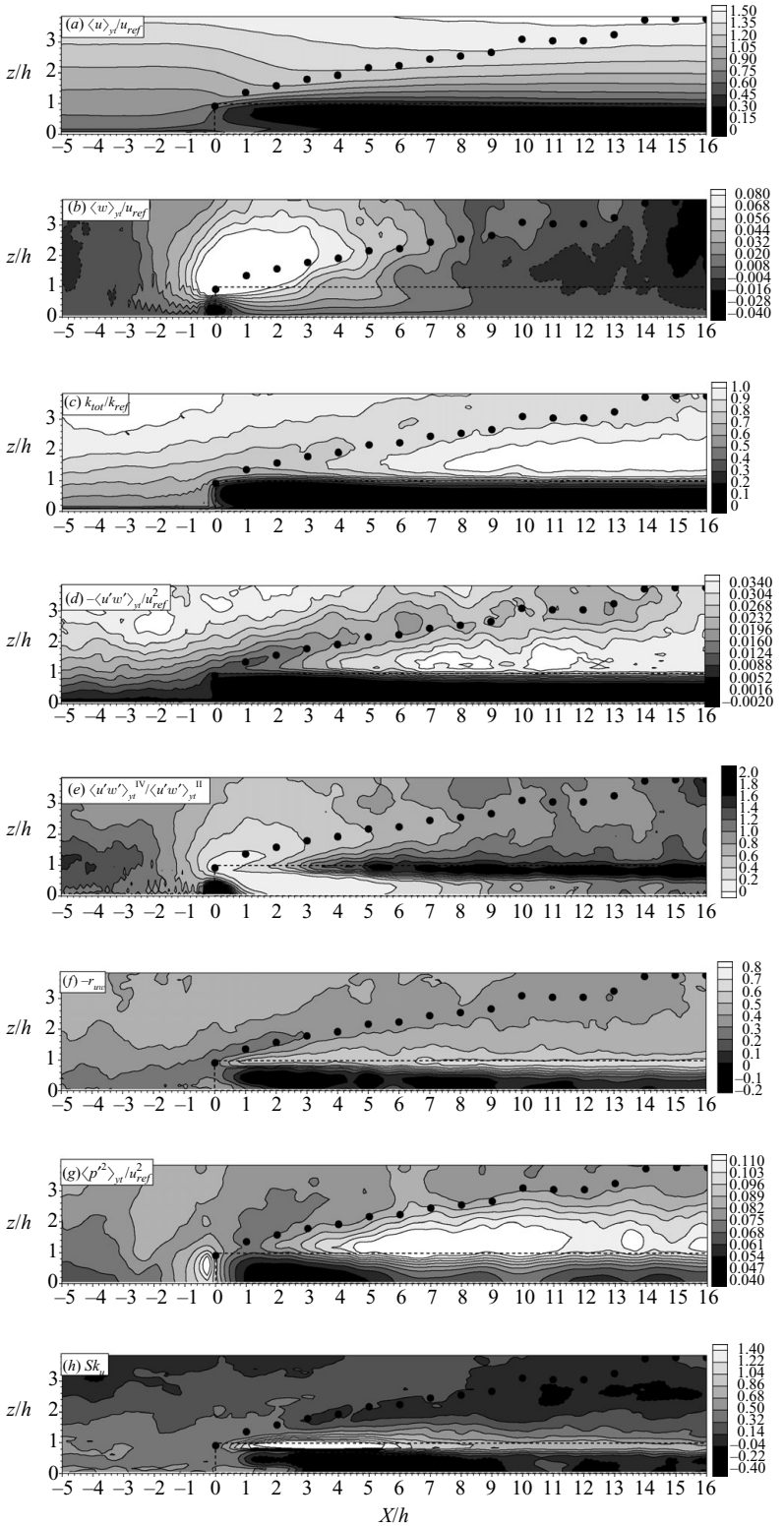

FIGURE 5. Same as figure 3 but for case 2 ($LAI = 5$).

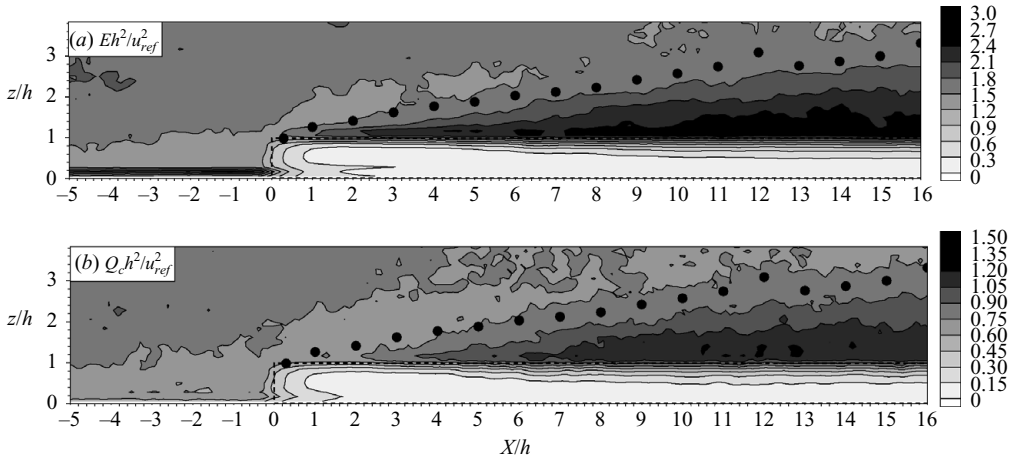

FIGURE 6. Vertical cross-section of the average enstrophy (a) and Q-criterion (b) fields for case 1 ($LAI = 2$). Both variables are normalized from the mean wind speed u_{ref} at $X = -8.5h$ and $z = 2h$. The dashed black line indicates the contour of the canopy and the black dots the upper limit of the IBL.

length of the adjustment region found here with $LAI = 5$ corresponds to $8L_c$, which is much larger than the estimate of Belcher *et al.* (2008), i.e. $3L_c$. As already mentioned for $LAI = 2$, part of this discrepancy may be explained by the inhomogeneity of the vertical foliage distribution in the present canopy.

3.2. *Mean enstrophy and Q-criterion fields*

Figure 6 presents x–z slices of time- and y-averaged enstrophy and Q-criterion fields. Since the cores of coherent structures are characterized by a local rotation rate larger than the strain rate, only the positive values of the Q-criterion variable were considered in the average, in order to identify the main regions in which coherent structures are the most intense or the most frequent. Looking at the average negative values of the Q-criterion would be of no interest here, as it would only highlight regions in which the strain rate is large, which are located within the lower part of the IBL. The enstrophy and Q-criterion exhibit similar behaviour. Both increase above the canopy in a growing layer confined within the IBL and exhibit a maximum at the canopy top. Both maxima are adjusted with the canopy from about $X = 8h$. The enstrophy increases directly from the canopy edge, while the Q-criterion starts to increase further downstream, from around $X = 2h$ to $X = 3h$. (Upstream of this location the strain rate at the canopy top is larger than the rotation rate.) Consequently, large coherent structures induced by the canopy in the adjustment region may be initiated around $X = 2h$, in relation with the quasi-adjustment of the shear length scale, L_s, at the canopy top, and are fully developed after $X = 8h$.

With a denser canopy (case 2), the enstrophy and Q-criterion develop more rapidly above the canopy (figure 7), as previously observed in § 3 with other turbulent statistical fields. Their magnitudes are also larger; coherent structures may therefore be more intense or more frequent and develop more rapidly from the edge. On the other hand, the enstrophy and Q-criterion decrease more rapidly with depth in the canopy and are slightly smaller, indicating that coherent structures penetrate less easily deep within the dense canopy.

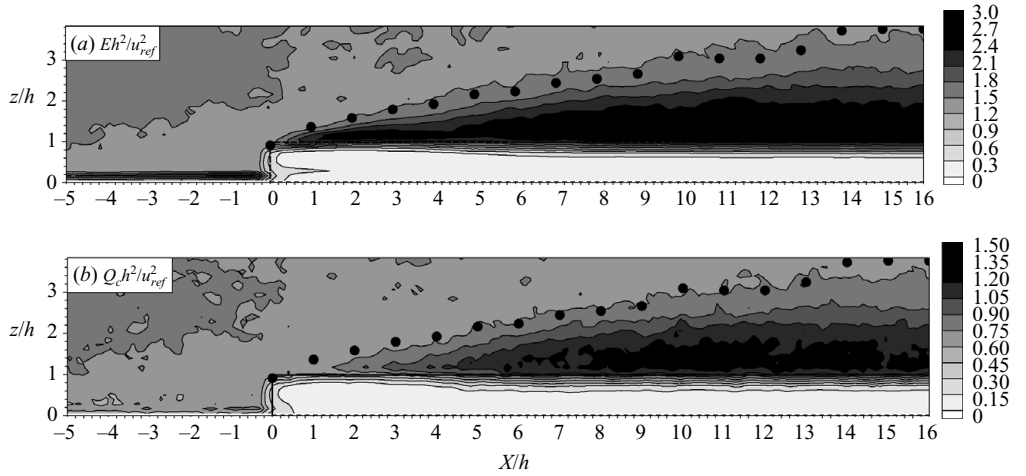

FIGURE 7. Same as figure 6 but for case 2 ($LAI = 5$).

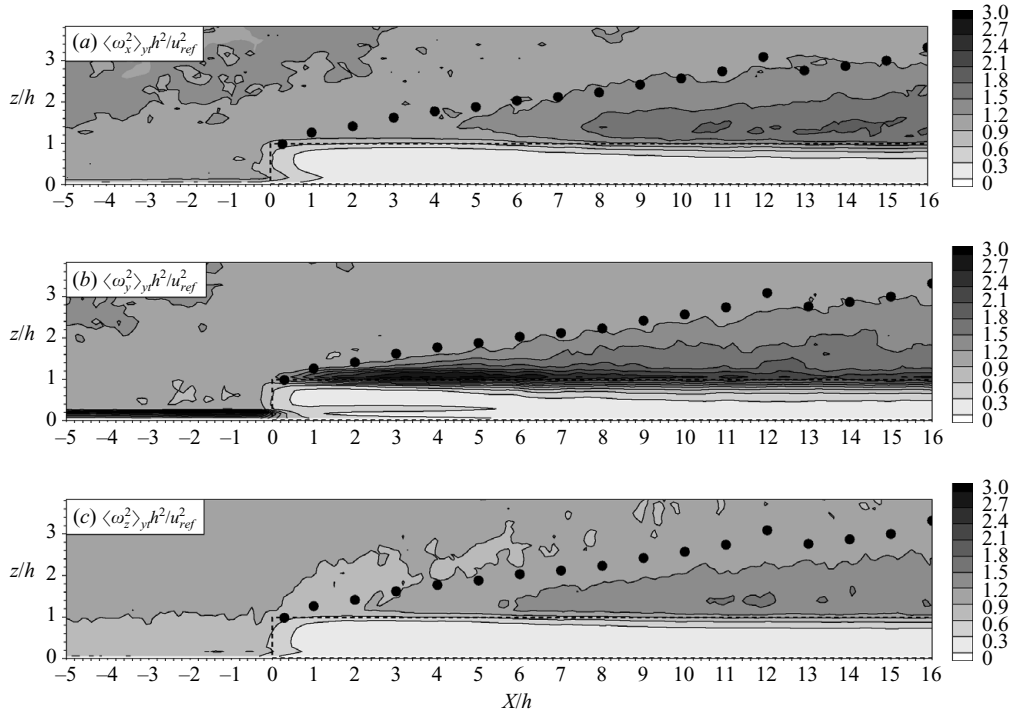

FIGURE 8. Vertical cross-section of the average square of the vorticity components in the streamwise (a), spanwise (b) and vertical (c) directions in case 1 ($LAI = 2$). Vorticity components are normalized from the mean wind speed u_{ref} at $X = -8.5h$ and $z = 2h$. The dashed black line indicates the contour of the canopy and the black dots the upper limit of the IBL.

The enstrophy is computed as the half-sum of the square of the three vorticity components of the flow $\langle\omega_x^2\rangle_{yt}$, $\langle\omega_y^2\rangle_{yt}$ and $\langle\omega_z^2\rangle_{yt}$ in the streamwise, spanwise and vertical directions, respectively. These three components are shown in figures 8 and 9 for the sparsest and densest canopies, respectively. Upwind from the canopy, their

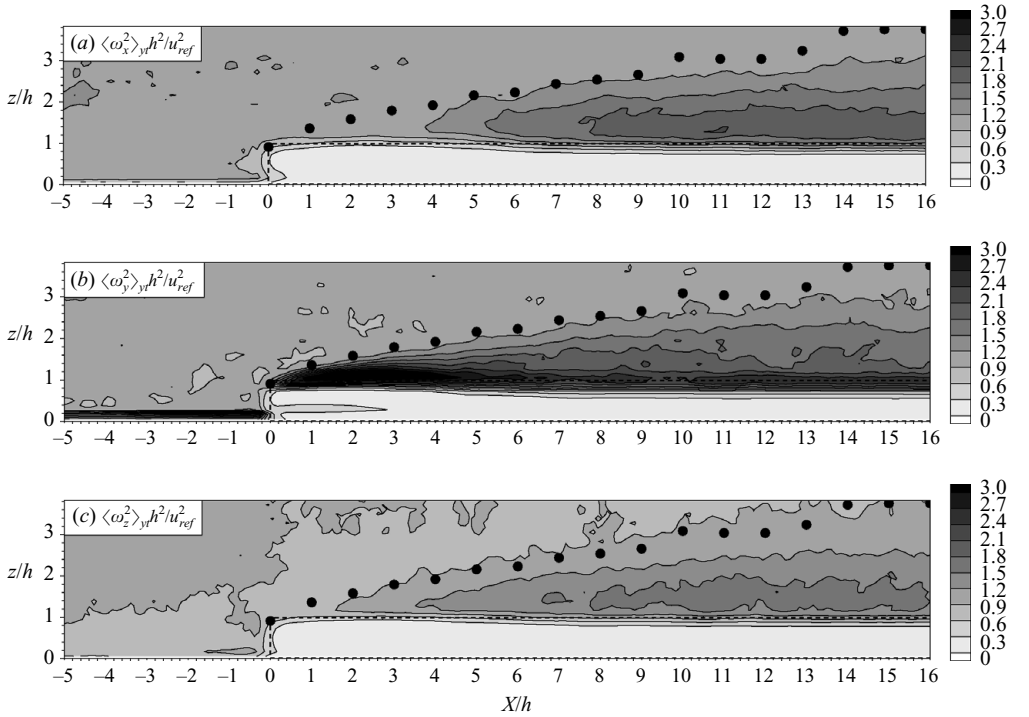

FIGURE 9. Same as figure 8 but for case 2 ($LAI = 5$).

magnitudes are roughly identical, with a slightly smaller value for the vertical component. Above the canopy, $\langle\omega_y^2\rangle_{yt}$ is always larger than $\langle\omega_x^2\rangle_{yt}$, followed by $\langle\omega_z^2\rangle_{yt}$, implying that coherent structures have a dominant transverse rotation rate, although $\langle\omega_y^2\rangle_{yt}$ includes a larger contribution from the mean shear ($\langle\partial u/\partial z\rangle_{yt}$). When the flow hits the canopy, $\langle\omega_y^2\rangle_{yt}$ first increases and reaches a maximum just above the top, in the region defined by $z = 1h$–$1.2h$ and $X = 3h$–$5h$ (for the sparsest canopy), before it slightly decreases further downstream. It then reaches its adjusted value, which is always larger than for the other two components. With a larger canopy density, the region of maximum $\langle\omega_y^2\rangle_{yt}$ is closer to the edge and more intense (figure 9*b*). The $\langle\omega_x^2\rangle_{yt}$ and $\langle\omega_z^2\rangle_{yt}$ components do not increase from the edge as $\langle\omega_y^2\rangle_{yt}$ does but from around $X = 6h$. They adjust at a faster rate, around $X = 10h$ near the canopy top. Unlike $\langle\omega_y^2\rangle_{yt}$, $\langle\omega_x^2\rangle_{yt}$ and $\langle\omega_z^2\rangle_{yt}$ are maximum not at the canopy top but just above the canopy, between $z = 1.2h$ and $z = 1.7h$. Within the canopy, the three vorticity components decrease very rapidly with depth, with slightly larger values for $\langle\omega_y^2\rangle_{yt}$.

The region in which $\langle\omega_y^2\rangle_{yt}$ is maximum (at the canopy top and $X = 3h$–$5h$ for the sparsest canopy), i.e. in which coherent structures are essentially transverse, coincides with the location of the EGZ and with an increase in pressure variance at the canopy top. Further downstream the transverse rotation rate is partly redistributed along the streamwise and vertical rotation directions. There is evidence for the presence of canopy-type coherent structures in this region, since the Q-criterion becomes positive there and since momentum exchange also starts to be dominated by sweep motions. These transverse vortices may therefore be viewed as the initial coherent structures induced by the canopy.

3.3. *Two-point correlations of velocity components*

Two-point correlations of velocity components provide information on the mean size and average topology of coherent structures. Streamwise, spanwise and vertical velocity isocorrelations and cross-correlations R_{11}, R_{22}, R_{33}, R_{13}, R_{12} and R_{23} (2.7) are computed using a reference point at the canopy top and a range of distances from the leading edge of the canopy. The analysis of the main characteristics of coherent structures after the forest leading edge is based here on the observation of three figures in parallel (figures 10–12). This allows us to limit repetitions in the structure description and give a continuing picture of the structure from the edge to the equilibrium region. The contours of R_{11}, R_{22}, R_{33} and R_{13} are shown in figures 10 and 11 in the x–z plane, and the contours of R_{12} and R_{23} are shown in figure 12 in the y–z plane.

Well downwind from the edge, at $X \geqslant 10h$, the shapes of the correlated areas are consistent with those previously observed over homogeneous canopies in wind-tunnel (Shaw *et al.* 1995), field (Raupach, Antonia & Rajagoplan 1991) and LES (Su *et al.* 2000; Dupont & Brunet 2008*b*) experiments. In the x–z plane with a downwind tilt from the horizontal R_{11} and R_{22} have a near-elliptical form (figure 10), while R_{33} is roughly circular in the three space directions with a slight elongation in the vertical (figure 11*a*). The well-correlated areas of R_{11}, and of R_{22} to a lesser extent, appear much larger than those of R_{33}. The reason is that u and v include contributions from large eddies coming from the atmosphere aloft (inactive turbulence), whereas w depends more on local flow properties and is therefore representative of more active turbulence, which is responsible for most of momentum transport (Raupach *et al.* 1996). The downwind tilt angles of R_{11} and R_{22} have been estimated along the x-axis in the same way as in Dupont & Brunet (2008*b*), i.e. by performing a linear regression on the height of the maximum in R_{11} and R_{22} in each vertical section, across a region between the reference point and the downwind point at which R_{11} and R_{22} become less than 0.2, respectively (figure 13). The slope angles deduced from R_{11} and R_{22} are similar and close to 20° (figure 13, at $X \geqslant 10h$), in good agreement with previous observations (Shaw *et al.* 1995). Within the canopy a region of negative correlation of R_{11} is present upstream from the reference point, indicating a recirculation region. Furthermore, the maximum of R_{11} occurs with a spatial shift reflecting a positive time delay from the treetop level. This shows that turbulent structures penetrating the canopy are inclined in the forward direction. Conversely, the maximum of R_{33} occurs with no time delay, which shows that perturbations in vertical velocity at treetop occur simultaneously at all levels within the canopy, due to the rapid diffusion of pressure fluctuations within the canopy (Raupach, Finnigan & Brunet 1989; Shaw & Zhang 1992). Since large values of u at the canopy top are usually associated with negative values of w, the negative contours of R_{13} (figure 11*b*) should be more representative of sweep motions than ejection motions; R_{13} contours indicate that the average structure shape associated with R_{11} contours is a sweep motion at the canopy top, preceded by an ejection, since R_{13} is negative at the reference point and positive upwind. Contours of R_{11} and R_{22} in the x–z plane do not represent the same part of the coherent structures, since u and v are not correlated in the x–z plane, as R_{12} is close to zero (figure not shown). In the y–z plane, contours of R_{12} and R_{23} indicate the presence of two counter-rotating streamwise vortices around the sweep motion at the canopy top and centred at about $Y = -1h$ and $Y = 1h$ (figure 12*a*), in agreement with the ensemble-averaged eddy structure observed from LES by Finnigan *et al.* (2009) over a homogeneous canopy. As stated in § 1.1, coherent structures over homogeneous canopies are characterized by an upstream head-down sweep-generating

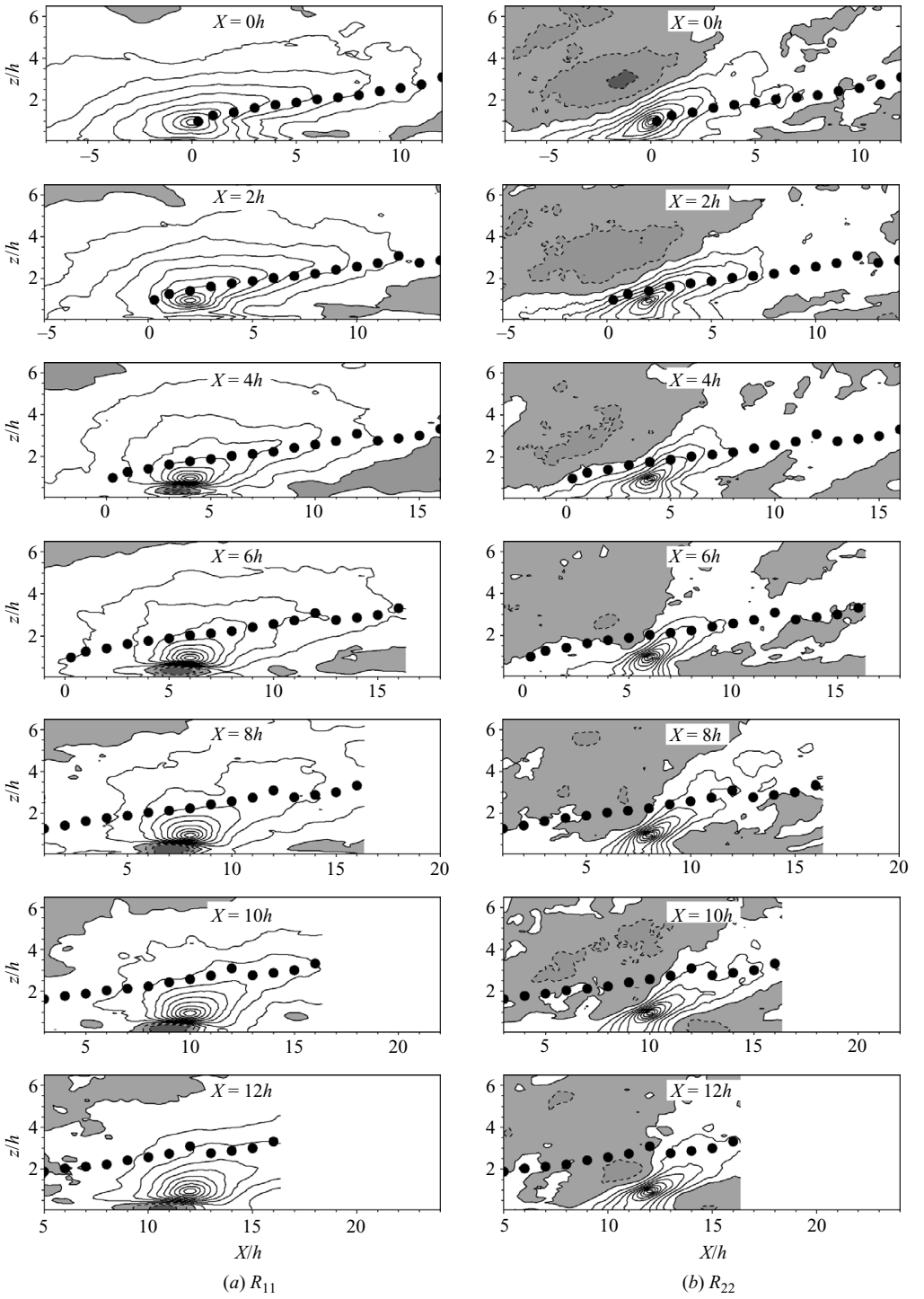

FIGURE 10. Contours of the average streamwise (*a*) and spanwise (*b*) velocity autocorrelation functions, R_{11} and R_{22}, respectively, in a streamwise cross-section at various distances from the forest leading edge in case 1 ($LAI = 2$). Contours are displayed from -0.2 to 0.9 with an interval of 0.1. Grey areas indicate negative values of correlations. The black dots indicate the upper limit of the IBL.

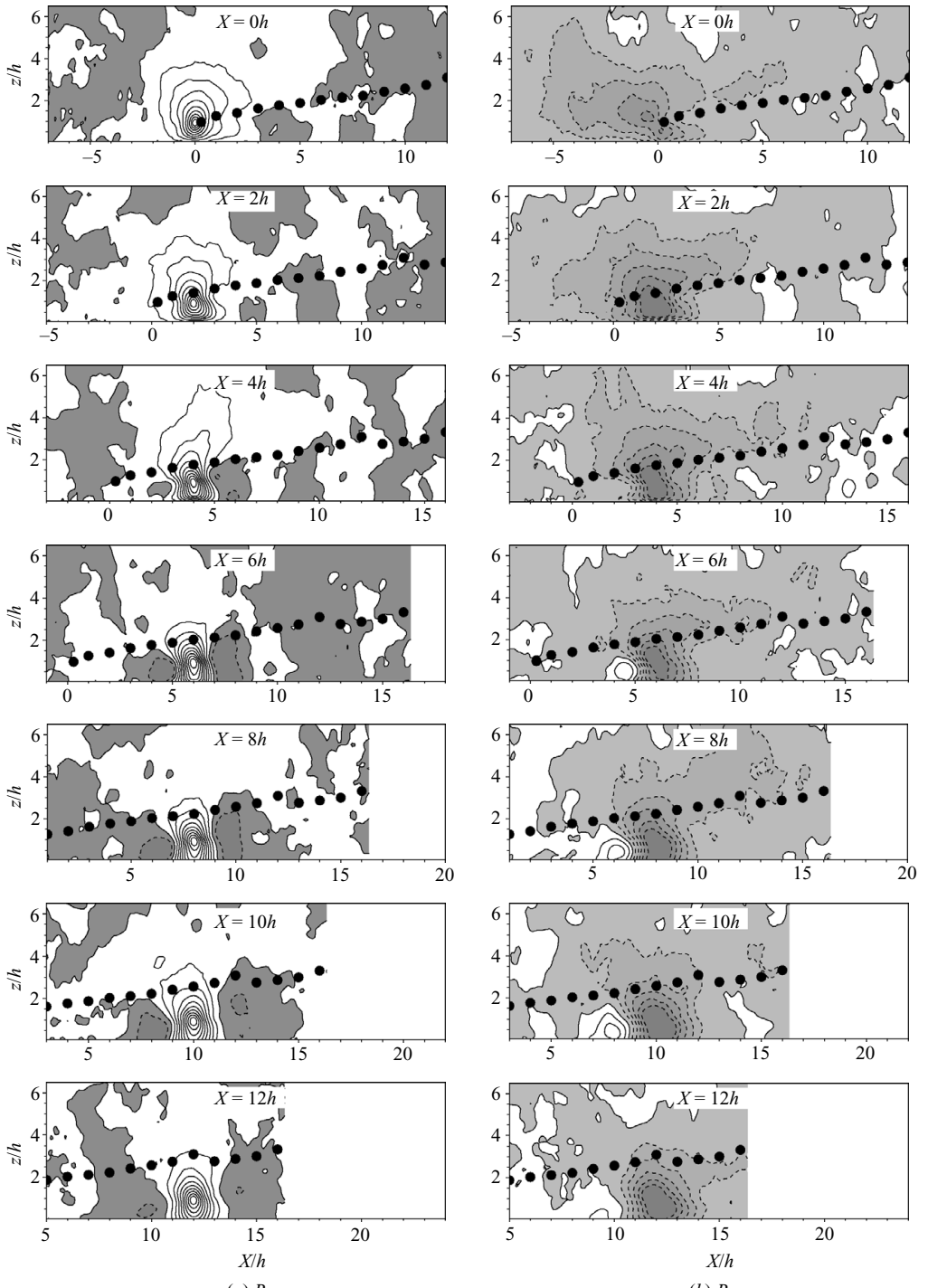

FIGURE 11. Same as figure 10 but for the vertical velocity autocorrelation R_{33} (*a*) and the cross-correlation R_{13} between the streamwise and the vertical velocities (*b*). Contours are displayed from −0.1 to 0.9 with an interval of 0.1 (*a*) and from −0.4 to 0.4 with an interval of 0.08 (*b*).

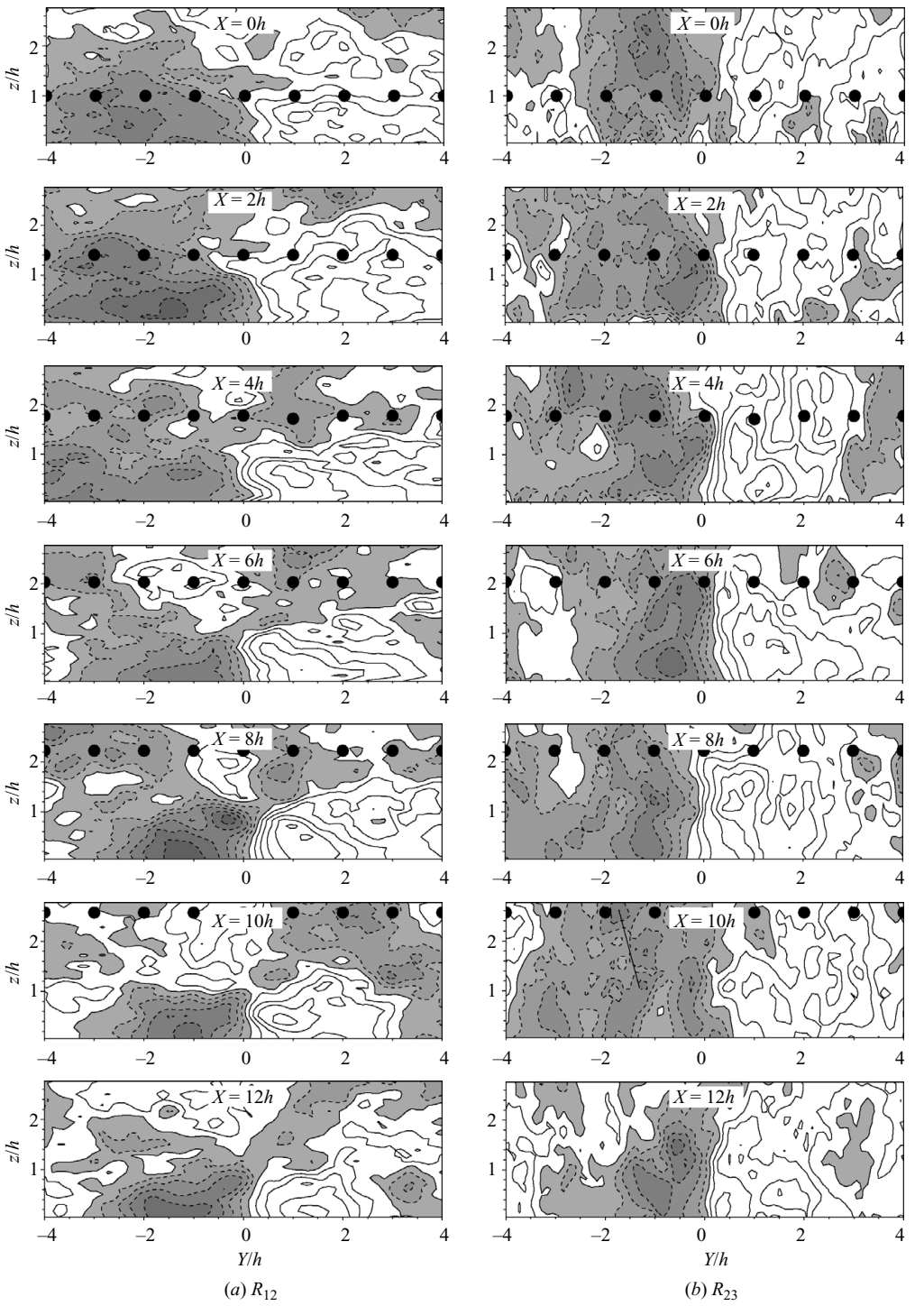

FIGURE 12. Contours of the average cross-correlation functions between the streamwise and spanwise velocities R_{12} (*a*) and between the spanwise and vertical velocities R_{23} (*b*), in spanwise cross-sections located at various distances from the forest leading edge in case 1 ($LAI = 2$). Contours are displayed from -0.5 to 0.5 with an interval of 0.1. Grey areas indicate negative values of correlations. The black dots indicate the upper limit of the IBL.

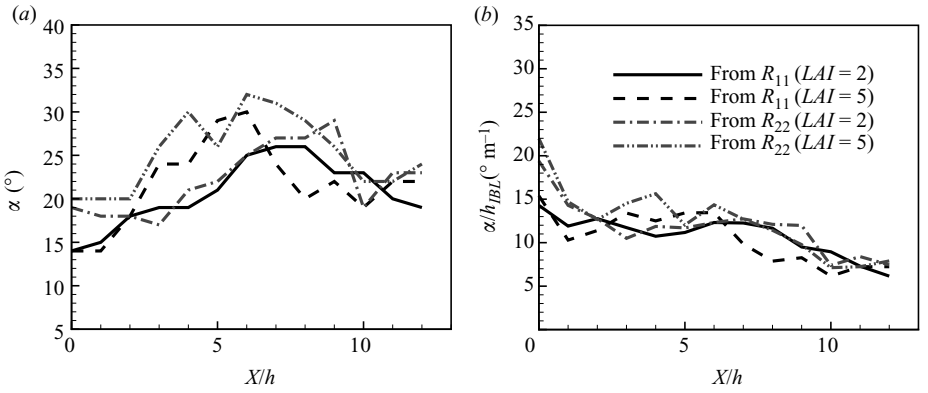

FIGURE 13. (*a*) Slope angle α of R_{11} and R_{22} in the streamwise direction downstream from the forest leading edge in cases 1 ($LAI = 2$) and 2 ($LAI = 5$); (*b*) is the same as (*a*), but α is normalized by the IBL depth, h_{IBL}.

hairpin vortex, i.e. with a pair of counter-rotating longitudinal vortices in the spanwise direction, superimposed on a downstream head-up ejection-generating hairpin vortex (Finnigan *et al.* 2009). Consequently, contours of R_{22} in the x–z plane may represent an ensemble average of the counter-rotating longitudinal vortices constituting the pair of hairpin vortices. As sweep motions dominate ejection motions at the canopy top, head-down vortices play a major role.

In the edge region, $X \leqslant 2h$, R_{11} and R_{22} already exhibit a near-elliptical shape further downstream (figure 10), but their contours and also those of R_{33} (figure 11*a*) extend within and above the canopy as well as in the IBL over larger streamwise and lateral distances than further downstream, meaning that structures in this region are much larger. The correlated area of R_{11} is especially larger upwind from the reference point, which may be the signature of strong wind gusts coming from the clearing and reaching the canopy top at its edge. The slope angle of R_{11} is about 15° (figure 13*a*), a value close to that of the IBL, since the contours of R_{11} are stretched along the top of the IBL (figure 10*a*). The angle of R_{22}, about 20°, is larger (figure 13*a*). Within the canopy, the negative correlated area observed in R_{11} further downstream is not yet present, and R_{33} is lower. In the y–z plane, the double-roller structure is not observed. Since the shear layer at the canopy top is not yet well developed in this region (L_s is larger than its equilibrium value), the structures associated with these correlated contours may be more representative of large structures coming from the upwind clearing than structures developing at the canopy top.

In the adjustment region ($2h < X < 10h$), the well-correlated areas of R_{11}, R_{22} and R_{33} are now essentially confined within the IBL (figures 10*a, b* and 11*a*). The slope angles of R_{11} and R_{22} are very similar; they both increase with increasing distance from the edge and reach a maximum around $X = 6h$–$7h$ before they decrease towards their adjusted value of 20° (figure 13*a*). Figure 13(*b*) shows the variations in the slope angles of R_{11} and R_{22} after the edge, normalized by the IBL height. It appears that both normalized slopes do not vary in the region $2h \leqslant X \leqslant 8h$, meaning that the increase of the structure slope observed here is related to the development of the IBL. Further downstream both normalized slopes decrease as the IBL still develops, while the structure slopes have adjusted. Within the canopy, the negative correlated area of R_{11} develops from about $X = 4h$ and reaches a maximum in magnitude at about $X = 6h$, associated with a positive correlated area of R_{13}. Additionally, R_{33} increases

within the canopy and starts to be surrounded by negative correlated regions at about $X = 4h$, suggesting that sweeps penetrate more easily and are surrounded by slight ejections. This feature is more marked around $X = 6h$. The negative peak of R_{11} in the sub-canopy coincides with the maximum in spanwise vorticity observed in § 4.1, corresponding to coherent structures with a dominant transverse vorticity component and, consequently, with recirculation regions within the canopy, characterized by a negative streamwise velocity. In the y–z plane, counter-rotating streamwise vortices surrounding sweep motion become visible from about $X = 6h$, while in the x–z plane, the width of the positive correlated area of R_{22} becomes smaller and better defined, which may indicate the presence of the first double-roller structures from the edge, characteristics of canopy turbulent structures. This feature is also confirmed by the development of the streamwise and vertical vorticity components in this region (figure 8*a* and *c*) and by the establishment of the shear layer at the canopy top (figure 4).

With increasing canopy density ($LAI = 5$; figure not shown), the correlated areas establish more rapidly from the edge, as was observed for the mean turbulence fields in § 3.1. Hence, canopy structures seem to develop closer to the edge in agreement with the faster establishment of the shear layer. The slope angles of R_{11} and R_{22} have a similar behaviour with increasing distance from the edge as for the sparser canopy but remain slightly larger and reach a maximum value closer to the edge, between $X = 5h$ and $X = 6h$, due to the faster-growing and deeper IBL that drives the slope angle of the structures from $X = 1h$–$6h$ (figure 13*b*).

3.4. *Separation length scale of coherent structures*

As stated in the introduction, coherent structures can be seen as occasional, large-amplitude excursions in time series of instantaneous turbulent variables. Several conditional techniques such as the wavelet transform exist to detect ramp-like signatures of coherent structures. Collineau & Brunet (1993*a*, *b*) demonstrated that the wavelet transform is a suitable tool for detecting coherent structures in the vicinity of vegetation canopies by decomposing time series into time and scale and by determining the location of the dominant structures in the time series. In order to analyse the variation of the length scale, l_i (where i is either 'u' or 'w'), and the separation length scale, Λ_i, of coherent structures with the distance from the edge, the wavelet transform technique was applied to instantaneous time series of the streamwise and vertical wind velocity components u and w, respectively, at various distances downwind from the leading edge of both canopies. The same methodology as in Brunet & Irvine (2000) and Dupont & Brunet (2008*b*), summarized in the Appendix, was used; Λ_i is estimated as $(TU_c)/N_i$ and l_i as $(U_c\Gamma_i)$, where N_i is the number of structures detected during time T, Γ_i the average structure time scale and U_c the convection velocity of the structures, which was assumed equal to $1.8\langle u\rangle_{yt}^{z=h}$ as suggested by Raupach *et al.* (1996). Figure 14 shows Λ_u and Λ_w normalized by the shear length scale, L_s, (figure 14*a*) and by the IBL depth, h_{IBL}, (figure 14*b*) and l_u and l_w normalized by L_s (figure 14*c*) and h_{IBL} (figure 14*d*).

For both canopies, Λ_w normalized by L_s appears adjusted with the canopy from about $X = 3h$, while l_w is adjusted about $2h$ further downstream. The opposite is visible when Λ_w is normalized by h_{IBL}. The rapid establishment of the shear layer from the edge (figure 4) explains the rapid adjustment of Λ_w, as the development of Kelvin–Helmhotlz instabilities that initiate coherent structures, and thus their separation distance, is driven by L_s. On the other hand, the adjustment of l_w requires a longer distance from the edge, of about $5h$–$6h$. In the region $3h \leqslant X \leqslant 6h$, l_w

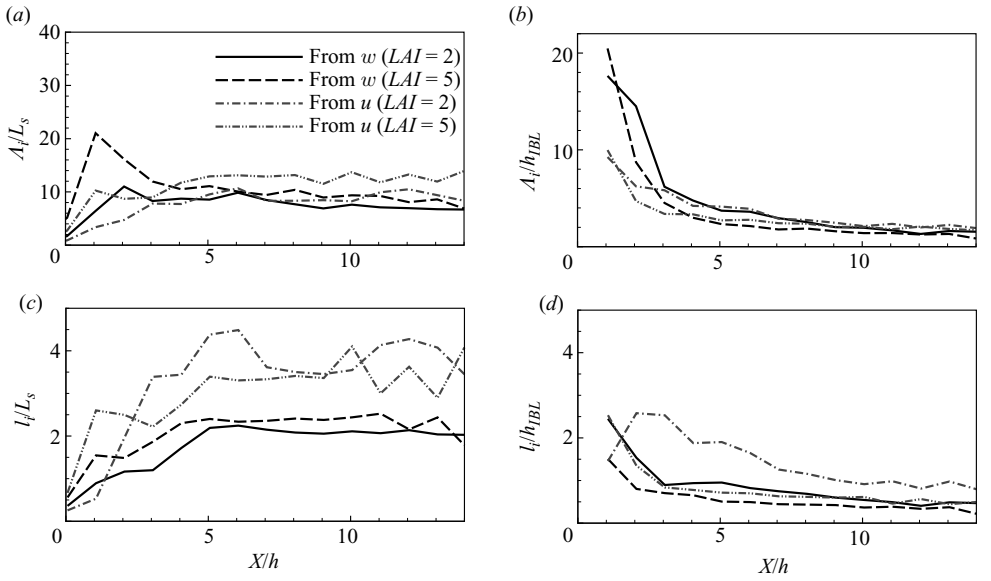

FIGURE 14. Separation distance Λ_i between two successive structures at the canopy top, normalized by the shear length scale L_s (*a*) and by the IBL depth, h_{IBL} (*b*), and length scale l_i for structures at the canopy top, normalized by L_s (*c*) and h_{IBL} (*d*), computed downwind of the forest leading edge from time series of u and w for the sparse ($LAI = 2$) and dense ($LAI = 5$) canopies.

scales with the depth of the IBL ($l_w/h_{IBL} \approx 1$). Hence, the adjustment distance of l_w corresponds to that over which the IBL has grown enough to allow the structures to be fully developed, as imposed by the depth of the canopy-top shear layer. This adjustment distance is also that required by the development of two counter-rotating streamwise vortices, i.e. about $6h$ (see § 3.3).

In the adjusted region, Λ_u and l_u appear about twice as large as Λ_w and l_w, respectively, for both canopies, whatever the normalization used, which is consistent but slightly less than the ratio of 3 observed by Brunet & Irvine (2000). This feature is explained by the fact that u includes contribution from large eddies coming from the atmosphere above, while w is more representative of the active turbulence. Furthermore, Λ_w/L_s ranges between 8 and 9 for both canopies in agreement with the 7–10 range identified by Raupach *et al.* (1996) from the plane mixing-layer analogy of canopy flow. Just behind the edge, Λ_w appears much larger than Λ_u when normalized by h_{IBL}, meaning that a large number of detected structures reaching the canopy have a negligible vertical wind velocity.

3.5. *Instantaneous fields*

The development of specific coherent eddies from the canopy leading edge is analysed in this section. For this purpose figures 15–18 present x–z slices of instantaneous streamwise wind velocity, perturbation pressure, enstrophy and Q-criterion, respectively, at 5 s intervals during a period of 30 s over the dense canopy ($LAI = 5$). Two coherent structures are tracked; they are localized in the figures by dashed circles referenced by letters A and B, respectively.

A $t = 0$ s, coherent structure A is already developed and localized around $X = 3.8h$. It is characterized by a slight recirculation within the canopy, a low pressure, a maximum in enstrophy just above the canopy and a small maximum of the Q-criterion. This

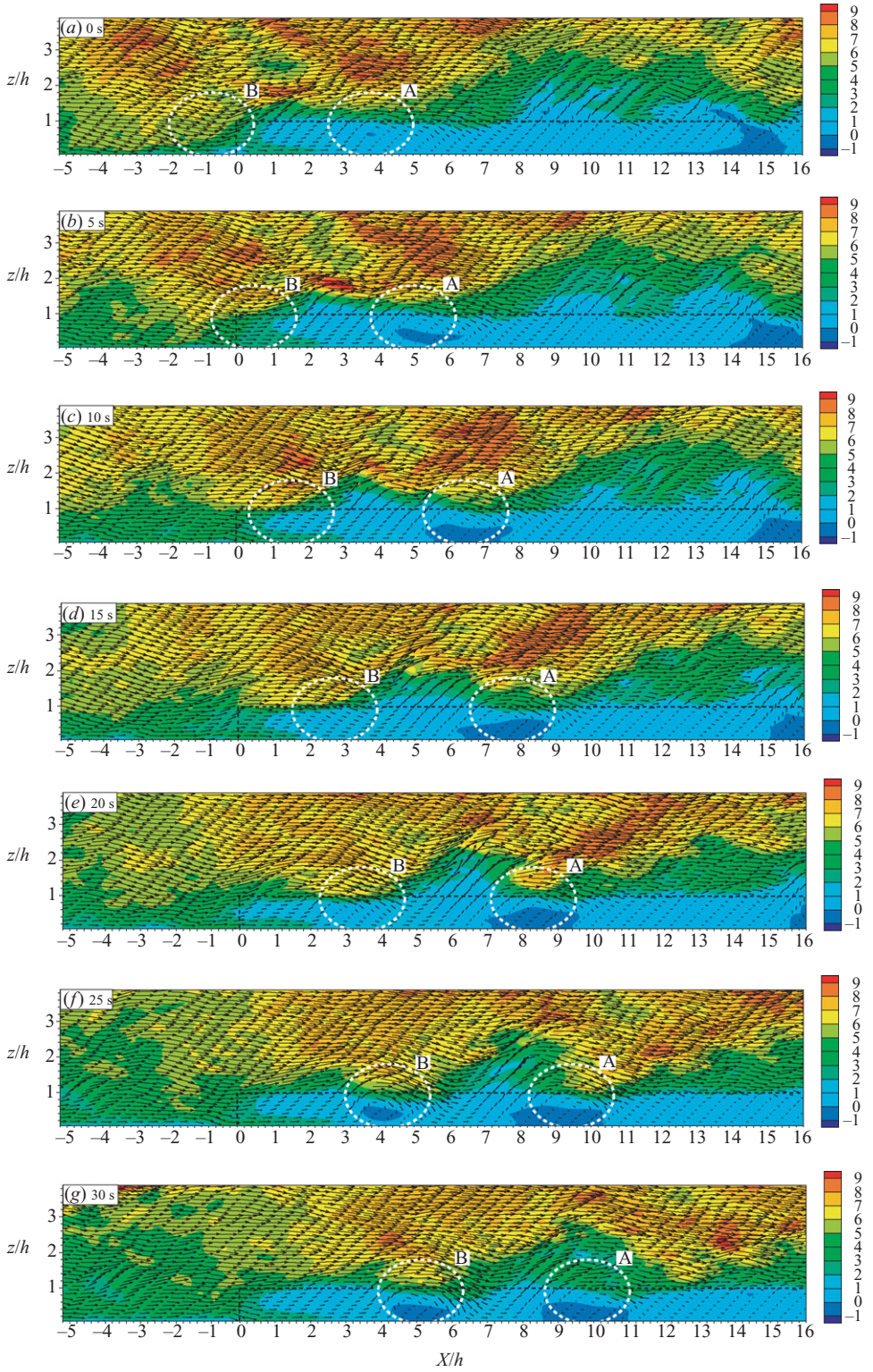

FIGURE 15. Streamwise cross-section of instantaneous streamwise wind velocity (background colour) and wind vectors at 5 s intervals during a period of 30 s (case 2, $LAI = 5$). The dashed circles identified by letters A and B track the development of two coherent structures. The dashed black line indicates the contour of the canopy.

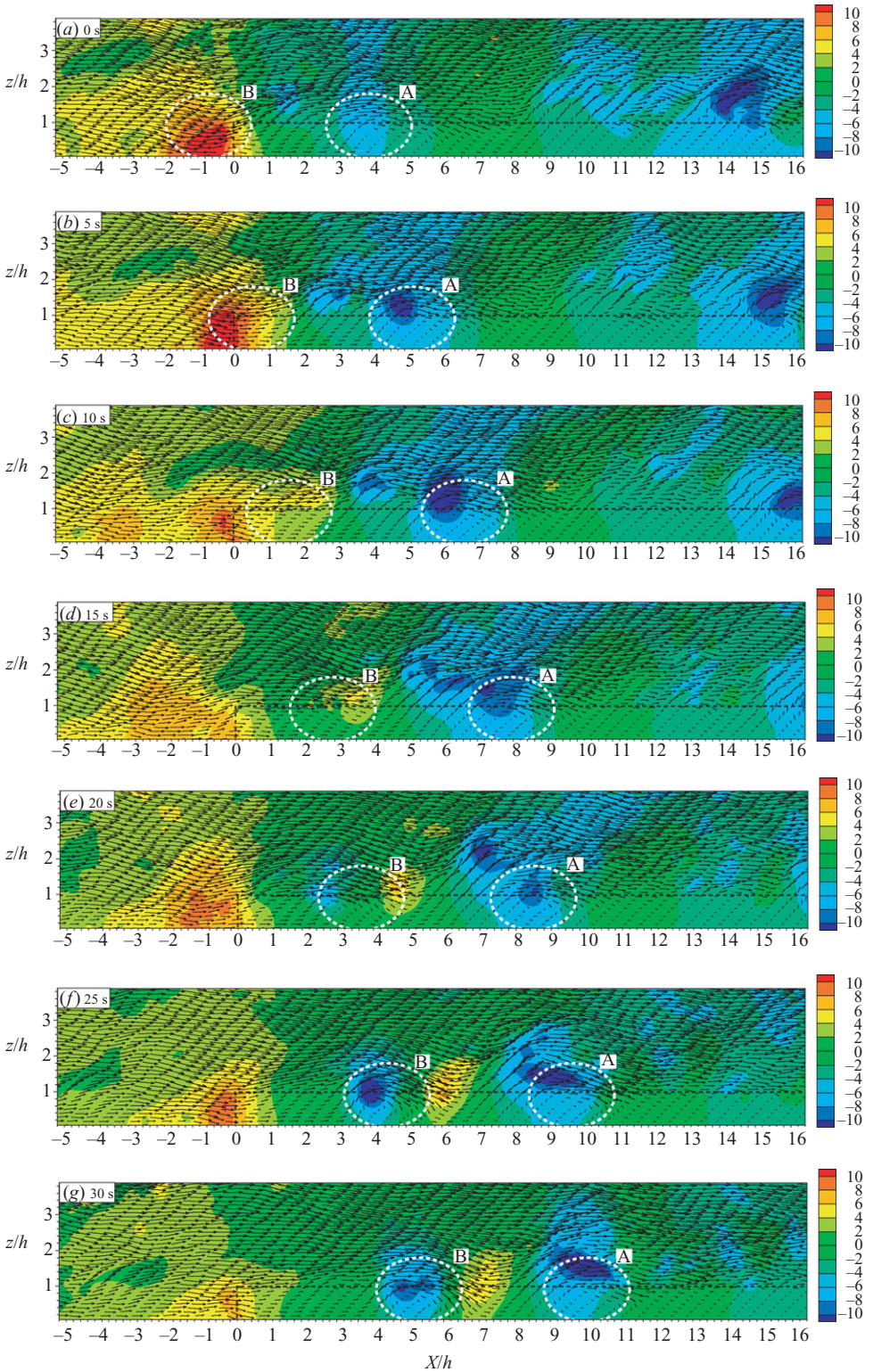

FIGURE 16. Same as figure 15, for the pressure perturbation.

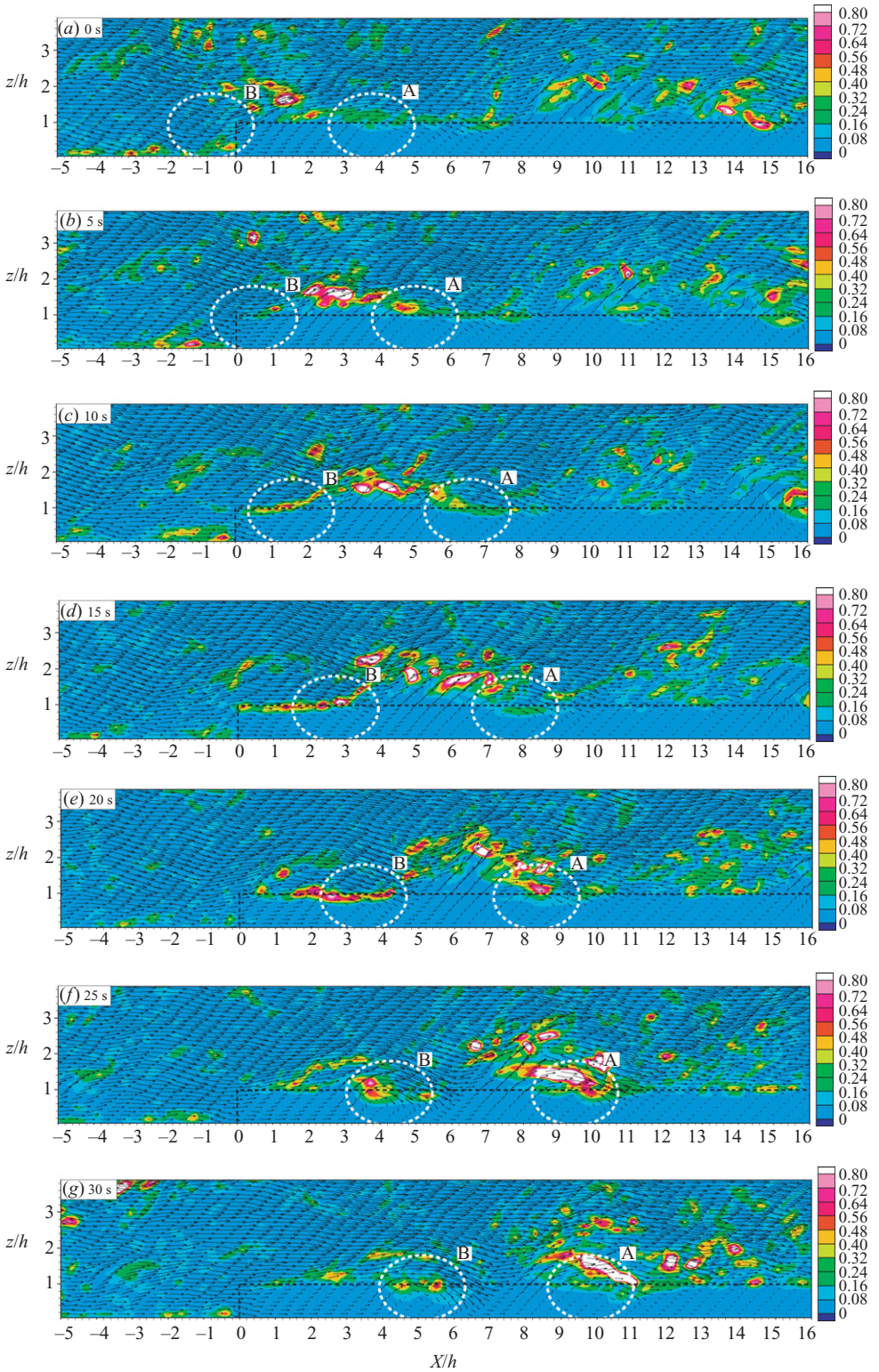

FIGURE 17. Same as figure 15, for the enstrophy.

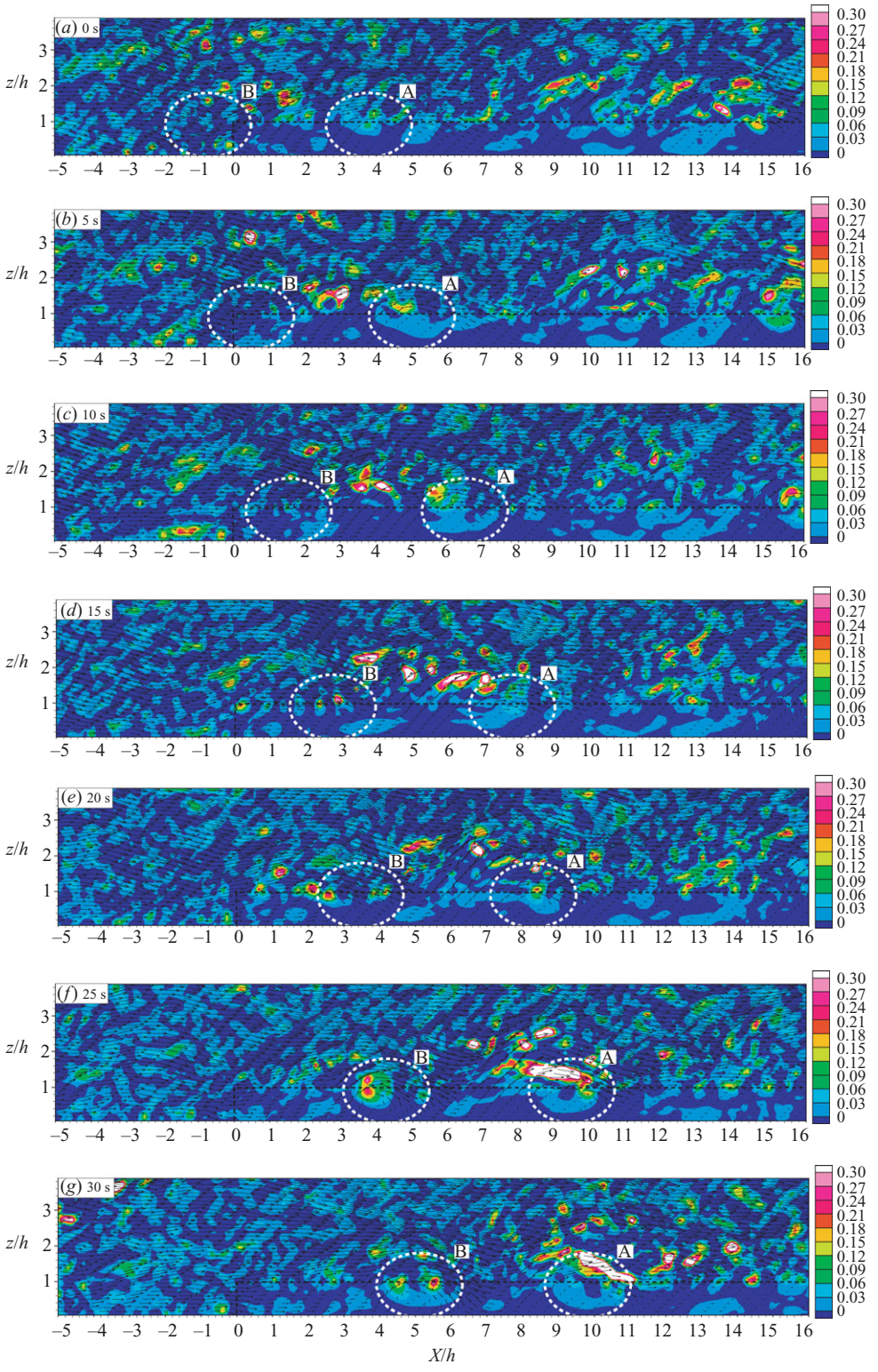

FIGURE 18. Same as figure 15, for the Q-criterion.

structure is transported by the flow and increases in intensity with a maximum enstrophy and Q-criterion at $t = 20$ s, around $X = 8h$. At this time, wind vectors indicate that the structure is essentially transverse with a clear recirculation within the canopy. The structure then interacts with other small structures coming from above and is transformed into a more complex structure with several less intense vortex cores as indicated by the enstrophy and Q-criterion maxima. This region is characterized by a low pressure.

At $t = 0$ s, coherent structure B is not yet developed. After a strong wind gust hits the canopy edge it seems to move parallel to the canopy top, down to about $X = 3.5h$ at $t = 20$ s. This gust contributes to increasing the skewness of the streamwise velocity as discussed in § 3. During the first 10 s, this gust is characterized by high pressure. High pressure is later located at the front of the gust, whereas a low-pressure maximum forms on its back ($t = 20$ s). The gust enstrophy increases at the canopy top, and the Q-criterion remains small but positive, indicating that the rotation rate of the flow is slightly larger than the strain rate. From $t = 25$ s, the gust starts to roll over around $X = 4h$ with the formation of a recirculation region within the canopy. The wind vectors indicate the formation of a transverse vortex, which is well defined at $t = 30$ s. The core of this vortex is characterized by a low pressure and a maximum in enstrophy and Q-criterion. A sweep motion can be seen on its downwind side at which pressure is maximum and an ejection motion on its upwind side at which pressure is minimum. The analysis of the wind velocity components in a spanwise slice (not shown here) suggests that the sweep motion induces the formation of a pair of counter-rotating longitudinal vortices, which have some similarities with the ensemble-averaged picture of coherent structures identified by Watanabe (2004) and Finnigan *et al.* (2009) from spatially averaged coherent structures but with a much more disturbed shape. The structure is transported by the flow and breaks down further downstream, around $X = 7h$, into smaller and less coherent structures at about $t = 45$ s (not shown). It takes structure B about 20 s to reach its maturity stage around $X = 4h$ and about an additional 20 s to decay around $X = 7h$. A rough estimate of the convection velocity of the structure from figure 15 confirms previous observations (Shaw *et al.* 1995) that the convection velocity, about 3.5 m s^{-1}, is roughly twice the mean streamwise velocity of the flow at the canopy top, about 1.8 m s^{-1}.

4. Discussion and conclusions

The main characteristics of the flow in the adjustment region downstream from the forest leading edge observed in § 3.1 are sketched in figure 19(*a*). Associated with this mean flow behaviour, a schematic average picture of the various stages of formation of coherent eddy structures from the forest leading edge is also presented (figure 19*b*), as deduced from the mean numerical fields of wind vorticity and spatial correlations of the wind velocity components analysed in the previous section. We first focus on the sparser canopy ($LAI = 2$):

(i) In the edge region, from $X = 0$ to about $2h$, a strong wind gust coming from the upwind clearing or aloft, and reaching the canopy shear layer, induces the development of an inflection point in the velocity profile at the canopy top, leading to the development of Kelvin–Helmholtz instabilities. At this stage, the wind gust moves parallel to the canopy top with a maximum velocity at its front and an average near-elliptical form with a downwind tilt from the horizontal close to that of the growing IBL that develops at the edge (figure 10). No large coherent structures induced by

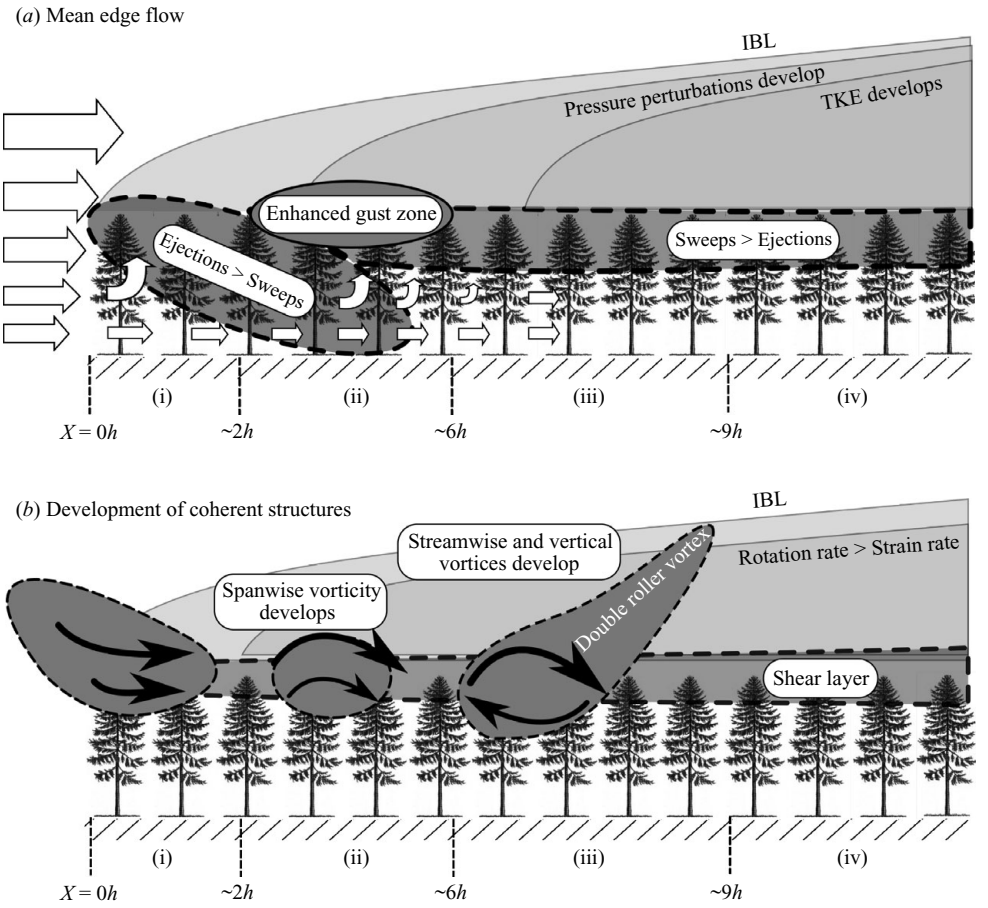

FIGURE 19. Idealized representation of the main characteristics of edge flow (*a*) and of the successive stages of development of coherent structures downwind from a forest leading edge (*b*) for a canopy with an LAI of about 2.

the canopy have completely formed yet, as indicated by the near-zero Q-criterion (figure 6*b*). This indeed means that the magnitudes of the flow rotation rate and strain rate are similar. Moreover, the momentum flux at the canopy top is dominated by ejection motions instead of sweep motions, which are currently observed over homogeneous canopies. This domination of ejection motions in the edge region is due to the penetration of turbulent structures within the canopy from the upwind side of the edge, which are hereafter advected vertically towards the canopy top when they are not totally dissipated by canopy drag. These ejection motions may also be responsible for the rapid increase in the efficiency of vertical turbulent transfer from the edge, as illustrated by the behaviour of r_{uw} (figure 3*f*).

(ii) Between about $X = 3h$ and $X = 5h$, the shear layer at the canopy top has already adjusted (figure 4) and induces the formation of transverse vortices through Kelvin–Helmholtz instabilities, as shown by the increase in the lateral component of wind vorticity (figure 8*b*). Furthermore, positive values of the Q-criterion appear around $X = 2h$ (figure 6*b*), meaning that the rotation rate becomes larger than the strain rate. Such rollers may therefore be considered as the first large coherent structures induced by the canopy behind the leading edge. At the beginning of their life, these structures

are essentially transverse, since the lateral component of wind vorticity is maximum between $X = 3h$ and $X = 5h$ (figure 8*b*) and larger than the other two. Contours of the streamwise wind velocity correlation, R_{11}, indicate that it reaches a negative maximum at mid-canopy height due to the recirculation induced by the presence of these transverse rollers. The positive time delay of the R_{11} maximum within the canopy indicates that these structures are slightly inclined when they penetrate the canopy (figure 10*a*). Due to the rapid adjustment of the shear length scale, L_s, the average distance between successive structures at the canopy top is also adjusted in this region, while the structure length scale still increases with the growing IBL up to about $5h$–$6h$, where the IBL is deep enough for structures to fully develop. In this region, the length scale of active turbulent structures is close to the IBL depth. The growth of turbulent structures is probably associated with processes of aggregation of close structures as observed from instantaneous fields (§ 3.5) as well as in mixing layers (Winant & Browand 1974; Dimotakis & Brown 1976). With the formation of coherent structures in this region, the ejection motions dominating vertical momentum exchange are progressively replaced by sweep motions from about $X = 3h$ (figure 3*e*) that contribute to maintain the large efficiency of vertical turbulent transfer at the canopy top, as illustrated by the behaviour of r_{uw} (figure 3*f*). The presence of these coherent structures is also responsible for the increase in the pressure variance at the canopy top (figure 3*g*) caused by the presence of regions of low and high pressure in the core and at the front of these structures, respectively. Additionally, the skewness of the streamwise velocity, Sk_u, reaches a maximum (figure 3*h*) corresponding to the EGZ observed by Raupach *et al.* (1987) from wind-tunnel measurements, where strong intermittent downward motions penetrate the canopy. Dupont & Brunet (2008*a*) suggested that the EGZ could be explained by the low turbulence levels in this region, which may emphasize the occasional presence of strong wind gusts coming from aloft or from the clearing. This indeed increases the skewness of the flow, whereas further downstream strong wind gusts are more 'diluted' in larger ambient turbulence. This assumption was reinforced by the observation of Dupont & Brunet (2008*a*) of a strong negative correlation between the canopy top Sk_u and TKE downwind from the leading edge.

(iii) Secondary instabilities, probably due to the strong wind shear at the canopy top, then destabilize the transverse coherent structures. They lead to an increase in vertical and streamwise vorticity components from around $X = 6h$ (figures 8*a* and 6*c*), but the transverse component still dominates the other two. In the transverse plane, two counter-rotating streamwise vortices start to be visible from the spatial cross-correlation between the streamwise and spanwise wind velocity components (figure 12*a*), which surround the sweep motion at the canopy top. This feature is in agreement with the schematic picture of coherent structures obtained by Finnigan *et al.* (2009) from an LES as an upstream head-down sweep-generating hairpin vortex superimposed on a downstream head-up ejection-generating hairpin vortex. In our case, the observed two counter-rotating streamwise vortices may result from the ensemble average of pairs of hairpin vortices, with the predominance of the head-down vortex, as sweep motions dominate ejection motions at the canopy top. This structure shape is further consistent with the location of maxima in the vertical and streamwise vorticity components, which are not at the canopy top as the spanwise component but slightly above it. Indeed, the lower base of the double-roller vortices may be characterized by a spanwise vortex at the canopy top, inducing a maximum in spanwise vorticity, while the downwind pair of counter-rotating vortices, characterized by large values of streamwise and vertical vortices, are positively inclined from the

horizontal. The separation distance and length scale of these structures are adjusted with the canopy (figure 14).

(iv) Further downstream, from about $X = 9h$, all turbulent variables have adjusted with the canopy and exhibit the well-known characteristics of homogeneous canopies. The initial transverse vortices located at a few canopy heights behind the edge have become complex three-dimensional vortices through the influence of instabilities, as is observed over homogeneous canopies. These structures later break down to smaller and less coherent structures and are replaced by other structures in formation.

In a denser canopy ($LAI = 5$) the development of coherent structure and of the IBL, as well as the adjustment of turbulent fields from the edge, are more rapid. The EGZ and the maximum of spanwise vorticity, and consequently the rollover of wind gusts, occur closer to the leading edge (figures 5*h* and 8*b*, respectively). Additionally, turbulent processes are enhanced in the adjustment region: the transverse rotation rate is larger, and the EGZ is more intense. A decrease in coherent-structure separation distance with increasing canopy density is observed, in agreement with Raupach *et al.* (1996) who predicted that the streamwise spacing of the dominant canopy eddies Λ_w is proportional to the shear length scale, L_s, since L_s decreases with increasing canopy density.

The schematic picture of coherent-structure formation described above reinforces the prediction of Raupach, Coppin & Legg (1986) and Raupach *et al.* (1996) that coherent structures over a vegetation canopy are generated through mechanisms similar to those acting in a plane mixing layer. It also confirms the suggestion of Morse *et al.* (2002) that the forest edge itself generates a plane mixing layer. While in plane mixing-layer flows the shear layer continuously decays, the shear layer at the canopy top adjusts at a few canopy heights from the edge and is further maintained by canopy drag (Nepf & Ghisalberti 2008). Compared with the schematic picture of large eddy formation over homogeneous canopies proposed by Finnigan & Brunet (1995) (figure 1), the main difference lies in the fact that the successive stages of coherent-structure development occur at relatively well-defined locations in the adjustment region after the leading edge, whereas they occur at random locations over homogeneous canopies.

This development of coherent structures from the forest leading edge may also be compared with the development of vortices simulated above the edge of a solid block (front-facing step flow) by Lesieur *et al.* (2003), as this case can be considered as the extreme case of an infinitely dense vegetation canopy. The main difference between the flow across a forest edge and that in a mixing layer or across a solid block is the presence in the edge adjustment region of a mean upward motion from the lower flow to the upper flow. This average upward motion brings up low values of TKE towards the flow interface (the canopy-top region here), which delays the development of the region of high TKE at the flow interface and therefore enhances the skewness of the streamwise wind velocity. Furthermore, the presence of a mean upward motion in the edge adjustment region may contribute, along with the background turbulence, to destabilize the initial transverse rollers. Consequently, the instantaneous topology of these structures, as observed from turbulent fields, are not as well-defined as in a mixing layer in which the inlet flow is usually laminar. However, the analysis of instantaneous fields shows that coherent structures appear as resulting from the 'branching' of tubes localized in region of low pressure in which their cores are characterized by high values of enstrophy and Q-criterion.

Although mesoscale structures were not considered in our simulation due to the limited vertical size of the computational domain, we believe in the conclusion that

the general picture of the mean flow and turbulent structures that comes out of this study would still be valid in a more developed neutral boundary layer. It has to be pointed out that these results apply to canopies with homogeneous foliage vertical distribution and a rather dense trunk space. For canopies with a more open trunk space such as in a maritime pine forest (Dupont & Brunet 2008*a*), turbulence edge flow should be more complicated.

We would like to thank the CAPS at the University of Oklahoma for providing the ARPS code. Computer simulations related to this work were performed on the EPHYSE cluster and on the NEC-SX8 at the Institut du Développement et des Ressources en Informatique Scientifique (IDRIS), Orsay, France. Thanks are expressed to the EPHYSE computing team (Patrick Moreau, Tovo Rabemanantsoa, Guy Pracros and Dr Mark R. Irvine) for their help with the cluster set-up. Dr Mark R. Irvine is also gratefully acknowledged for his help on the wavelet transform tool. Finally, we thank anonymous reviewers for their helpful comments.

Appendix. Ramp-signal detection with wavelet transform

The wavelet transform was used to detect ramp-like coherent structures in time series, following the same approach as Collineau & Brunet (1993*a*, *b*) and Brunet & Irvine (2000). The continuous wavelet transform of a signal, $h(t)$, is defined as

$$T_p(a,b) = \frac{1}{a^p}\int_{-\infty}^{\infty} h(t)g\left(\frac{t-b}{a}\right)\mathrm{d}t, \tag{A 1}$$

where $g(t)$ is the wavelet function; a is the wavelet scale; b is position translation; p is a normalization factor equal to 1 here; and $T_p(a,b)$ represents the wavelet coefficients.

As the normalized wavelet variance spectra $W_p(a)$ represents the distribution of energy along the scales (or wavelet dilatation) a, its peak should correspond to the scale of coherent structures:

$$W_p(a) = \int_{-\infty}^{\infty} |T_p(a,b)|^2\,\mathrm{d}b. \tag{A 2}$$

The wavelet transform was applied to instantaneous vertical and streamwise velocity time series with the following methodology:

(i) Wavelet transforms were computed from Haar wavelet over 30 min data runs sampled at 33 Hz, which were simulated by the model at the canopy top.

(ii) The representative scale of coherent structures was deduced from the wavelet variance spectra (peak scale).

(iii) Since the Mhat detection function crosses the zero line when a coherent structures is detected (Collineau & Brunet 1993 *b*), the previous peak Haar scale was converted to the corresponding Mhat scale, and wavelet coefficients were calculated for the characteristic scale of coherent structures with the Mhat wavelet.

(iv) The number of 'zero crosses' in the detection function was then counted to determine the average temporal separation of coherent structures in the total time period and therefore their frequency.

REFERENCES

Asner, G. P., Scurlock, J. M. O. & Hicke, J. A. 2003 Global synthesis of leaf area index observations: implications for ecological and remote sensing studies. *Global Ecol. Biogeogr.* **12** (3), 191–205.

Baldocchi, D. D. & Meyers, T. P. 1988 Turbulence structure in a deciduous forest. *Boundary-Layer Meteorol.* **43**, 345–364.

Belcher, S. E., Finnigan, J. J. & Harman, I. N. 2008 Flows through forest canopies in complex terrain. *Ecol. Appl.* **18** (6), 1436–1453.

Belcher, S. E., Jerram, N. & Hunt, J. C. R. 2003 Adjustment of a turbulent boundary layer to a canopy of roughness elements. *J. Fluid Mech.* **488**, 369–398.

Bou-Zeid, E., Meneveau, C. & Parlange, M. B. 2004 Large-eddy simulation of neutral atmospheric boundary layer flow over heterogeneous surfaces: blending height and effective surface roughness. *Water Resour. Res.* **40** (2), W02505.

Brunet, Y. & Irvine, M. R. 2000 The control of coherent eddies in vegetation canopies: streamwise structure spacing, canopy shear scale and atmospheric stability. *Boundary-Layer Meteorol.* **94** (1), 139–163.

Cassiani, M., Katul, G. G. & Albertson, J. D. 2008 The effects of canopy leaf area index on airflow across forest edges: large-eddy simulation and analytical results. *Boundary-Layer Meteorol.* **126** (3), 433–460.

Chen, J. M. T., Novak, M. D. & Adams, R. 1995 A wind tunnel study of turbulent air flow in forest clearcuts. In *Wind and Trees* (ed. M. P Coutts & J. Grace), pp. 71–97. Cambridge University Press.

Collineau, S. & Brunet, Y. 1993*a* Detection of turbulent coherent motions in a forest canopy. Part 1. Wavelet analysis. *Boundary-Layer Meteorol.* **65** (4), 357–379.

Collineau, S. & Brunet, Y. 1993*b* Detection of turbulent coherent motions in a forest canopy. Part 2. Time-scales and conditional averages. *Boundary-Layer Meteorol.* **66** (1–2), 49–73.

Comte, P., Lesieur, M. & Fouillet, Y. 1989 Coherent structures of mixing layers in large-eddy simulation. In *Topological Fluid Dynamics* (ed. H. K. Moffatt & A. Tsinober). Cambridge University Press, 649–658.

Comte, P., Lesieur, M. & Lamballais, E. 1992 Large-scale and small-scale stirring of vorticity and a passive scalar in a 3-d temporal mixing layer. *Phys. Fluids* A **4** (12), 2761–2778.

Cucitore, R., Quadrio, M. & Baron, A. 1999 On the effectiveness and limitations of local criteria for the identification of a vortex. *Eur. J. Mech.* B **18** (2), 261–282.

Dimotakis, P. E. & Brown, G. L. 1976 The mixing layer at high Reynolds number: large structure dynamics and entrainment. *J. Fluid Mech.* **78**, 535–560.

Dubief, Y. & Delcayre, F. 2000 On coherent-vortex identification in turbulence. *J. Turbul.* **1**, 011.

Dupont, S. & Brunet, Y. 2008*a* Edge flow and canopy structure: a large-eddy simulation study. *Boundary-Layer Meteorol.* **126**, 51–71.

Dupont, S. & Brunet, Y. 2008*b* Influence of foliar density profile on canopy flow: a large-eddy simulation study. *Agric. Forest Meteorol.* **148**, 976–990.

Dupont, S., Brunet, Y. & Finnigan, J. J. 2008 Large-eddy simulation of turbulent flow over a forested hill: validation and coherent structure identification. *Quart. J. R. Meteorol. Soc.* **134**, 1911–1929.

Dwyer, M. J., Patton, E. G. & Shaw, R. H. 1997 Turbulent kinetic energy budgets from a large-eddy simulation of airflow above and within a forest canopy. *Boundary-Layer Meteorol.* **84** (1), 23–43.

Farge, M. & Schneider, K. 2006 Wavelets: application to turbulence. In *Encyclopedia of Mathematics Physics* (ed. J.-P. Françoise, G. Naber & T. S. Tsun), pp. 408–420. Elsevier.

Finnigan, J. 2000 Turbulence in plant canopies. *Annu. Rev. Fluid Mech.* **32**, 519–571.

Finnigan, J. J. & Brunet, Y. 1995 Turbulent airflow in forests on flat and hilly terrain. In *Wind and Trees* (ed. M. P. Coutts & J. Grace), pp. 3–40. Cambridge University Press.

Finnigan, J. J. & Shaw, R. H. 2000 A wind-tunnel study of airflow in waving wheat: an EOF analysis of the structure of the large-eddy motion. *Boundary-Layer Meteorol.* **96** (1–2), 211–255.

Finnigan, J. J., Shaw, R. H. & Patton, E. G. 2009 Turbulence structure above a vegetation canopy. *J. Fluid Mech.* In press.

Flesch, T. K. & Wilson, J. D. 1999 Wind and remnant tree sway in forest cutblocks. Part 1. Measured winds in experimental cutblocks. *Agric. Forest Meteorol.* **93** (4), 229–242.

Gao, W., Shaw, R. H. & Paw U, K. T. 1989 Observation of organized structures in turbulent flow within and above a forest canopy. *Boundary-Layer Meteorol.* **47**, 349–377.

Gash, J. H. C. 1986 Observations of turbulence downwind of a forest–heath interface. *Boundary-Layer Meteorol.* **36**, 227–237.

Ghisalberti, M. & Nepf, H. M. 2002 Mixing layers and coherent structures in vegetated aquatic flows. *J. Geophys. Res.* **107** (C2), 3011.

Haller, G. 2005 An objective definition of a vortex. *J. Fluid Mech.* **525**, 1–26.

Irvine, M. R., Gardiner, B. A. & Hill, M. K. 1997 The evolution of turbulence across a forest edge. *Boundary-Layer Meteorol.* **84** (3), 467–496.

Jeong, J. & Hussain, F. 1995 On the identification of a vortex. *J. Fluid Mech.* **285**, 69–94.

Judd, M. J., Raupach, M. R. & Finnigan, J. J. 1996 A wind tunnel study of turbulent flow around single and multiple windbreaks. Part 1. Velocity fields. *Boundary-Layer Meteorol.* **80** (1–2), 127–165.

Kanda, M. & Hino, M. 1994 Organized structures in developing turbulent-flow within and above a plant canopy, using a large-eddy simulation. *Boundary-Layer Meteorol.* **68** (3), 237–257.

Katul, G. G., Schieldge, J., Hsieh, C. I. & Vidakovic, B. 1998 Skin temperature perturbations induced by surface layer turbulence above a grass surface. *Water Resour. Res.* **34** (5), 1265–1274.

Lee, X. 2000 Air motion within and above forest vegetation in non-ideal conditions. *Forest Ecol. Manage.* **135** (1–3), 3–18.

Lesieur, M., Begou, P., Briand, E., Danet, A., Delcayre, F. & Aider, J. L. 2003 Coherent-vortex dynamics in large-eddy simulations of turbulence. *J. Turbul.* **4**, 016.

Liu, J., Chen, J. M., Black, T. A. & Novak, M. D. 1996 E-epsilon modelling of turbulent air flow downwind of a model forest edge. *Boundary-Layer Meteorol.* **77** (1), 21–44.

Lu, C. H. & Fitzjarrald, D. R. 1994 Seasonal and diurnal variations of coherent structures over a deciduous forest. *Boundary-Layer Meteorol.* **69**, 43–69.

Morse, A. P., Gardiner, B. A. & Marshall, B. J. 2002 Mechanisms controlling turbulence development across a forest edge. *Boundary-Layer Meteorol.* **103** (2), 227–251.

Nepf, H. & Ghisalberti, M. 2008 Flow and transport in channels with submerged vegetation. *Acta Geophys.* **56** (3), 753–777.

Nieveen, J. P., El-Kilani, R. M. M. & Jacobs, A. F. G. 2001 Behaviour of the static pressure around a tussock grassland–forest interface. *Agric. Forest Meteorol.* **106** (4), 253–259.

Patton, E. G., Shaw, R. H., Judd, M. J. & Raupach, M. R. 1998 Large-eddy simulation of windbreak flow. *Boundary-Layer Meteorol.* **87** (2), 275–306.

Paw, K. T., Brunet, Y., Collineau, S., Shaw, R. H., Maitini, T., Qiu, J. & Hipps, L. 1992 On coherent structures in turbulence above and within agricultural plant canopies. *Agric. Forest Meteorol.* **61** (1–2), 55–68.

Pénelon, T., Calmet, I. & Mironov, D. V. 2001 Micrometeorological simulations over a complex terrain with submeso: a model study using a novel pre-processor. *Intl J. Environ. Pollut.* **16**, 583–602.

Qiu, J., Paw, U. K. & Shaw, R. H. 1995 Pseudo-wavelet analysis of turbulence patterns in three vegetation layers. *Boundary-Layer Meteorol.* **72** (1–2), 177–204.

Quine, C. P., Coutts, M. P., Gardiner B. & Pyatt, D. G. 1995 Forests and wind: management to minimize damage. In *Forestry Commission Bulletin 114*. (ed. B. Gardiner), HMSO Publications Centre.

Raupach, M. R., Antonia, R. & Rajagoplan, S. 1991 Rough-wall turbulent boundary layers. *Appl. Mech. Rev.* **44**, 1–25.

Raupach, M. R., Bradley, E. F. & Ghadiri, H. 1987 A wind tunnel investigation into aerodynamic effect of forest clearings on the nesting of Abbott's Booby on Christmas Island. *Tech Rep.* CSIRO Centre for Environmental Mechanics.

Raupach, M. R., Coppin, P. A. & Legg, B. J. 1986 Experiments on scalar dispersion within a plant canopy, Part 1. The turbulence structure. *Boundary-Layer Meteorol.* **35**, 21–52.

Raupach, M. R., Finnigan, J. J. & Brunet, Y. 1989 Coherent eddies and turbulence in vegetation canopies. In *Fourth Australian Conf. on Heat and Mass Transfer*. Christchurch, New Zealand.

Raupach, M. R., Finnigan, J. J. & Brunet, Y. 1996 Coherent eddies and turbulence in vegetation canopies: the mixing-layer analogy. *Boundary-Layer Meteorol.* **78** (3–4), 351–382.

Raynor, G. S. 1971 Wind and temperature structure in a coniferous forest and a contiguous field. *Forest Sci.* **17**, 351–363.

Rogers, M. M. & Moser, R. D. 1994 Direct simulation of a self-similar turbulent mixing layer. *Phys. Fluids* **6** (2), 903–923.

Schneider, K. & Farge, M. 2003 Extraction of coherent vortex tubes in a 3d mixing layer. In *Tubes, Sheets and Singularities in Fluid Dynamics* (ed. K. Bajer & H. H. Moffat), pp. 211–216. Kluwer.

Schneider, K., Farge, M., Pellegrino, G. & Rogers, M. M. 2005 Coherent vortex simulation of three-dimensional turbulent mixing layers using orthogonal wavelets. *J. Fluid Mech.* **534**, 39–66.

Shaw, R. H., Brunet, Y., Finnigan, J. J. & Raupach, M. R. 1995 A wind tunnel study of air flow in waving wheat: two-point velocity statistics. *Boundary-Layer Meteorol.* **76** (4), 349–376.

Shaw, R. H., Finnigan, J. J., Patton, E. G. & Fitzmaurice, L. 2006 Eddy structure near the plant canopy interface. In *26th Conf. on Boundary Layers and Turbulence*. San Diego, California.

Shaw, R. H., Hartog, D. & Neumann, H. H. 1988 Influence of foliar density and thermal stability on profiles of Reynolds stress and turbulence intensity in a deciduous forest. *Boundary-Layer Meteorol.* **45**, 391–409.

Shaw, R. H. & Schumann, U. 1992 Large-eddy simulation of turbulent-flow above and within a forest. *Boundary-Layer Meteorol.* **61** (1–2), 47–64.

Shaw, R. H. & Zhang, X. J. 1992 Evidence of pressure-forced turbulent-flow in a forest. *Boundary-Layer Meteorol.* **58** (3), 273–288.

Shen, S. H. & Leclerc, M. Y. 1997 Modelling the turbulence structure in the canopy layer. *Agric. Forest Meteorol.* **87** (1), 3–25.

Su, H. B., Shaw, R. H. & Paw, U. K. T. 2000 Two-point correlation analysis of neutrally stratified flow within and above a forest from large-eddy simulation. *Boundary-Layer Meteorol.* **94** (3), 423–460.

Su, H. B., Shaw, R. H., Paw, U. K. T., Moeng, C. H. & Sullivan, P. P. 1998 Turbulent statistics of neutrally stratified flow within and above a sparse forest from large-eddy simulation and field observations. *Boundary-Layer Meteorol.* **88** (3), 363–397.

Turner, B. J., Leclerc, M. Y., Gauthier, M., Moore, K. E. & Fitzjarrald, D. R. 1994 Identification of turbulence structures above a forest canopy using a wavelet transform. *J. Geophys. Res.* **99** (D1), 1919–1926.

Watanabe, T. 2004 Large-eddy simulation of coherent turbulence structures associated with scalar ramps over plant canopies. *Boundary-Layer Meteorol.* **112** (2), 307–341.

Winant, C. D. & Browand, F. K. 1974 Vortex pairing: the mechanism of turbulent mixing-layer growth at moderate Reynolds number. *J. Fluid Mech.* **63**, 237–255.

Xue, M., Droegemeier, K. K. & Wong, V. 2000 The Advanced Regional Prediction System (ARPS) – a multi-scale nonhydrostatic atmospheric simulation and prediction model. Part 1. Model dynamics and verification. *Meteorol. Atmos. Phys.* **75** (3–4), 161–193.

Xue, M., Droegemeier, K. K., Wong, V., Shapiro, A. & K., Brewster 1995 *ARPS Version 4.0 User's Guide*. Center for Analysis and Prediction of Storms, University of Oklahoma.

Xue, M., Droegemeier, K. K., Wong, V., Shapiro, A., Brewster, K., Carr, F., Weber, D., Liu, Y. & Wang, D. 2001 The Advanced Regional Prediction System (ARPS) – a multi-scale nonhydrostatic atmospheric simulation and prediction tool. Part 2. Model physics and applications. *Meteorol. Atmos. Phys.* **76** (3–4), 143–165.

Yang, B., Morse, A. P., Shaw, R. H. & Paw, U. K. T. 2006*a* Large-eddy simulation of turbulent flow across a forest edge. Part 2. Momentum and turbulent kinetic energy budgets. *Boundary-Layer Meteorol.* **121** (3), 433–457.

Yang, B., Raupach, M. R., Shaw, R. H., Tha, K., Paw, U. & Morse, A. P. 2006*b* Large-eddy simulation of turbulent flow across a forest edge. Part 1. Flow statistics. *Boundary-Layer Meteorol.* **120** (3), 377–412.